Enhancer of zeste homolog 2 (*Ezh2*) controls bone formation and cell cycle progression during osteogenesis in mice

Received for publication, March 19, 2018, and in revised form, June 12, 2018 Published, Papers in Press, June 13, 2018, DOI 10.1074/jbc.RA118.002983

Amel Dudakovic[‡§], Emily T. Camilleri[‡], Christopher R. Paradise[¶‖], Rebekah M. Samsonraj[‡], Martina Gluscevic[¶], Carlo Alberto Paggi[**], Dana L. Begun[‡], Farzaneh Khani[‡], Oksana Pichurin[‡], Farah S. Ahmed[‡], Ranya Elsayed[‡‡], Mohammed Elsalanty[‡‡], Meghan E. McGee-Lawrence[§§¶¶], Marcel Karperien[**], Scott M. Riester[‡], Roman Thaler[‡], Jennifer J. Westendorf[‡§], and Andre J. van Wijnen[‡§1]

From the [‡]Department of Orthopedic Surgery, the [§]Department of Biochemistry and Molecular Biology, the [¶]Mayo Clinic Graduate School of Biomedical Sciences, and the [‖]Center for Regenerative Medicine, Mayo Clinic, Rochester, Minnesota 55905, the [**]Department of Developmental BioEngineering, University of Twente, 7522 NB Enschede, Netherlands, the [‡‡]Department of Oral Biology, Augusta University, Augusta, Georgia 30912, and the Departments of [§§]Cellular Biology and Anatomy and [¶¶]Orthopedic Surgery, Medical College of Georgia, Augusta University, Augusta, Georgia 30912

Edited by Xiao-Fan Wang

Epigenetic mechanisms control skeletal development and osteoblast differentiation. Pharmacological inhibition of the histone 3 Lys-27 (H3K27) methyltransferase enhancer of zeste homolog 2 (EZH2) in WT mice enhances osteogenesis and stimulates bone formation. However, conditional genetic loss of *Ezh2* early in the mesenchymal lineage (*i.e.* through excision via *Prrx1* promoter–driven Cre) causes skeletal abnormalities due to patterning defects. Here, we addressed the key question of whether *Ezh2* controls osteoblastogenesis at later developmental stages beyond patterning. We show that *Ezh2* loss in committed pre-osteoblasts by Cre expression via the osterix/*Sp7* promoter yields phenotypically normal mice. These Ezh2 conditional knock-out mice (Ezh2 cKO) have normal skull bones, clavicles, and long bones but exhibit increased bone marrow adiposity and reduced male body weight. Remarkably, *in vivo* *Ezh2* loss results in a low trabecular bone phenotype in young mice as measured by micro-computed tomography and histomorphometry. Thus, *Ezh2* affects bone formation stage-dependently. We further show that *Ezh2* loss in bone marrow–derived mesenchymal cells suppresses osteogenic differentiation and impedes cell cycle progression as reflected by decreased metabolic activity, reduced cell numbers, and changes in cell cycle distribution and in expression of cell cycle markers. RNA-Seq analysis of *Ezh2* cKO calvaria revealed that the cyclin-dependent kinase inhibitor *Cdkn2a* is the most prominent cell cycle target of *Ezh2*. Hence, genetic loss of *Ezh2* in mouse pre-osteoblasts inhibits osteogenesis in part by inducing cell cycle changes. Our results suggest that *Ezh2* serves a bifunctional role during bone formation by suppressing osteogenic lineage commitment while simultaneously facilitating proliferative expansion of osteoprogenitor cells.

Mineralization of fetal tissues to form a bony skeleton is restricted to the later stages of gestation, and expression of bone-specific genes remains silenced during the earlier stages of embryogenesis. Silencing of genes and their regulatory regions is mediated by the tightly controlled organization of promoters and enhancers into nucleosomes, the fundamental units of chromatin (1, 2). Condensation of chromosomal loci in heterochromatin silences gene expression and occurs concomitant with post-translational modifications of histone N termini. One of the major mechanisms for heterochromatin formation is through trimethylation of histone 3 at lysine 27 (H3K27me3)[2] (3). The polycomb-repressive complex 2 (PRC2), which contains three structural proteins and the catalytic subunit enhancer of zeste homolog 2 (EZH2), catalyzes the mono-, di-, and trimethylation of H3K27. Enhancer of zeste homolog 1 (EZH1) can also serve as the catalytic subunit within the PRC2 complex and may also suppress gene expression, albeit by different mechanisms (3–5). Methylation of H3K27me3 is reversible by three histone demethylases, JHDM1D, KDM6A, and KDM6B (6). Hence, deposition and retention of H3K27me3 marks reflect the dynamic balance in the activities of opposing enzymes.

Epigenetic mechanisms play a critical role during skeletal development and osteoblast differentiation (2, 7–13). In addition, the epigenomic landscape of differentiating osteoblasts

This work was supported, in whole or in part, by National Institutes of Health Grants R01 AR049069 (to A. v. W.), R01 AR68103 (to J. J. W.), F32 AR066508 (to A. D.), and T32 AR056950 (to D. L. B.). This work was also supported by William H. and Karen J. Eby and the charitable foundation in their names. M. K. is founder and shareholder of Hy2Care B.V. The content is solely the responsibility of the authors and does not necessarily represent the official views of the National Institutes of Health.

This article contains Tables S1–S3 and Figs. S1 and S2.

RNA-Seq data were deposited in the Gene Expression Omnibus (GEO) of the National Institute for Biotechnology Information under accession number GSE111245.

[1] To whom correspondence should be addressed: Depts. of Orthopedic Surgery and Biochemistry and Molecular Biology, Mayo Clinic, 200 First St. SW, Rochester, MN 55905. Tel.: 507-293-2105; Fax: 507-284-5075; E-mail: vanwijnen.andre@mayo.edu.

[2] The abbreviations used are: H3K27me3, histone 3 Lys-27 trimethylation; H3K27, histone 3 Lys-27; PRC2, polycomb-repressive complex 2; μCT, micro-computed tomography; AMSC, adipose-derived mesenchymal stem cell; BMSC, bone marrow–derived mesenchymal stem cell; CON, control; BV, bone volume; TV, total volume; Ad, adenovirus; qPCR, quantitative PCR; real-time reverse transcription-quantitative PCR; MTS, 3-(4,5-dimethylthiazol-2-yl)-5-(3-carboxymethoxyphenyl)-2-(4-sulfophenyl)-2H-tetrazolium; αMEM, α-minimal essential medium; IGV, Interactive Genome Viewer; RPKM, reads/kilobase pair/million mapped reads; cKO, conditional knock-out.

has been documented in considerable detail (14–17). Several recent studies from our group have demonstrated that *Ezh2* and other epigenetic regulators play a critical role during mesenchymal lineage commitment and osteoblast differentiation (18–25). It has been established that *Ezh2* expression is significantly down-regulated during osteogenic commitment of human adipose-derived stem cells (AMSCs) (26, 27). Furthermore, loss or inhibition of EZH2 was shown to enhance osteogenic and inhibit adipogenic differentiation of AMSCs (26), human bone marrow–derived mesenchymal stem cells (BMSCs) (28), and MC3T3 mouse pre-osteoblasts (29). Mechanistically, EZH2 suppresses the expression of osteogenic genes and ligand-dependent signaling pathways (*e.g.* WNT, PTH, and BMP2) to favor adipogenic differentiation (26, 28–32). Importantly, three studies have shown that inhibition of EZH2 prevents bone loss that is associated with estrogen depletion *in vivo* (29, 33, 34). In addition, one of these studies also reported bone anabolic effects of EZH2 inhibition in mice (29).

With the exception of *Ezh1*, mice completely lacking expression of any of the PRC2 components are not viable (18). Thus, studies have assessed tissue-restricted genetic loss of *Ezh2* in the mesoderm (35), neural crest (36), mesenchymal stem cells (26, 35, 37), and chondrocytes (38). Loss of *Ezh2* in the mesoderm and neural crest causes embryonic lethality, whereas loss of this epigenetic enzyme in the mesenchyme produces viable mice that have several skeletal abnormalities, including craniosynostosis, clinodactyly, shortened limbs, and reduced bone volume. The loss of *Ezh2* in cartilage does not result in a significant phenotype, but dual loss of *Ezh1* and *Ezh2* severely impairs skeletal development (38). A similar phenotype was observed with the loss of EED, a structural component of the PRC2 complex (39), suggesting that both EZH1 and EZH2 require the PRC2 complex for their function.

In this study, we assessed the role of *Ezh2* in osteoblast differentiation and function. We show that conditional *Ezh2* loss in osteoblast precursors permits normal patterning and development but shows a remarkable trabecular bone phenotype reflected by reduced bone volume in young animals. Mechanistic assessment of this phenotype indicates that loss of bone is due to cytostatic effects on osteoprogenitor cells. The latter finding indicates that beyond the known biological role of *Ezh2* in suppressing osteogenic differentiation, it has a novel positive function in early stages of bone formation by supporting pre-osteoblast proliferation.

Results

Loss of Ezh2 in bone results in phenotypically normal mice

Our laboratory and others have demonstrated that conditional loss of *Ezh2* in the mesenchyme (*Ezh2* cKO^{Prrx1}) results in several developmental defects (*e.g.* shorted limbs, craniosynostosis, and clinodactyly) (26, 37). A subset of these phenotypic changes are easily understood as skeletal patterning defects that may result from the well-known activation of the *Prrx1* driver in the limb bud stage (40). However, to gain insight into the specific role of *Ezh2* in the osteoblast lineage and bone, *Ezh2*$^{flox/flox}$ mice were bred with *Osx-Cre* mice (41) to generate control (CON, *Ezh2*$^{wt/wt}$*: Osx-Cre*) and conditional knockout animals (*Ezh2* cKO^{Osx}, *Ezh2*$^{flox/flox}$*: Osx-Cre*). Loss of *Ezh2* in osteoblasts results in animals that are indistinguishable from CON mice (Fig. 1*a*). In addition, X-ray analysis revealed normal skeletal formation in *Ezh2* cKO^{osx} animals (Fig. 1*b*). Weight assessment of female mice at 3, 8, and 12 weeks of age did not reveal any differences between CON and *Ezh2* cKO^{osx} animals (Fig. 1*c*). However, *Ezh2* cKO^{Osx} male animals have slightly lower total body mass compared with CON mice at the earlier time points (3 and 8 weeks of age). Micro-computed tomography (μCT) analysis of male and female mice did not reveal any changes in the structure of the skulls (Fig. 1, *d* and *e*) or abnormalities of the clavicles (Fig. 1*f*). Thus, with the exception of minor changes in weights of young male mice, the loss of *Ezh2* in osteoblasts (in *Ezh2*$^{flox/flox}$*: Osx-Cre* mice) results in phenotypically normal mice.

Bone-specific loss of Ezh2 results in a low trabecular bone phenotype in young animals

To assess the effects of *Ezh2* loss on bone quality, μCT analysis was performed near proximal tibial epiphysis (trabecular bone) and tibial mid-shaft (cortical bone) of a fraction of male mice exhibiting similar weights at several stages of life (3, 8, and 12 weeks of age). Assessment of cortical bone demonstrates that there are no major differences between *Ezh2* cKO^{osx} and CON mice (Table S1). A minor reduction in cortical porosity is observed at 8 weeks in *Ezh2* cKO^{Osx} animals, which is statistically significant with a moderate level of confidence ($p < 0.05$). Analysis of trabecular bone reveals several quantitatively modest changes in bone parameters at 3 weeks of age (Table S2 and Fig. 2*a*). A reduction in trabecular bone volume (BV/TV), trabecular number, and connectivity density is observed in *Ezh2* cKO mice. Although the reduction in these bone parameters is numerically modest, it is significant at an adequate confidence level ($p < 0.05$). We also observe an apparent increase in trabecular spacing upon bone-specific loss of *Ezh2*, but this trend is not statistically significant ($p > 0.05$). Interestingly, no significant differences in trabecular bone parameters are observed at 8 weeks (Table S2 and Fig. 2*b*) and 12 weeks (Table S2 and Fig. 2*c*) of age between CON and *Ezh2* cKO^{Osx} animals. Histomorphological analysis was performed on femora derived from 3-week old male mice (Fig. 3). Von Kossa–McNeal (*a*) and Goldner's trichrome (*b*) staining of the distal femora demonstrate that the growth plate and cartilage morphologies are similar between CON and *Ezh2* cKO animals. However, Goldner's trichrome staining of the femora mid-shafts reveals that cKO animals exhibit enhanced bone marrow adiposity (*c*). Similar to μCT analysis at 3 weeks of age, histomorphometric analysis of distal femora shows a reduction in trabecular bone volume (BV/TV) with the loss of *Ezh2* in osteoblasts ($p < 0.05$) (*d*). The change in bone volume is accompanied by a reduction in osteoblasts surface per bone surface, osteoclast surface per bone surface, and number of osteoclasts per bone perimeter ($p < 0.05$ in all cases). Although we observed an apparent decrease in the osteoblasts surface per bone surface in adult cKO mice, these numerical changes do not reach significance ($p > 0.05$) (Fig. S1). Yet, reductions in osteoclast surface per bone surface remained lower in *Ezh2* cKO mice at 12 weeks of age ($p < 0.05$). Thus, whereas the deletion of *Ezh2* in osteoblasts does not alter

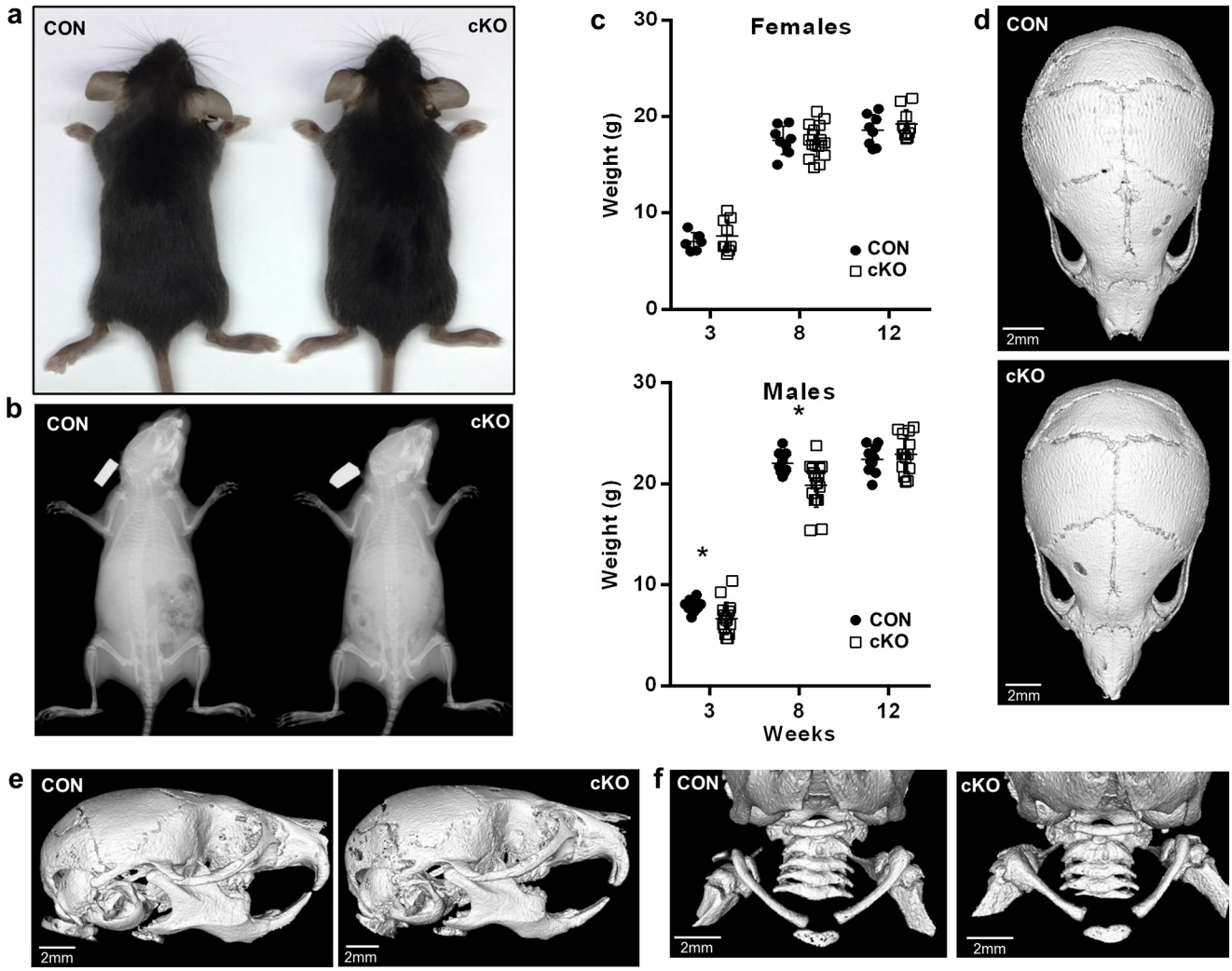

Figure 1. Bone-specific loss of *Ezh2* results in phenotypically normal mice. *a–c*, images (4 weeks, female) (*a*), X-ray analysis (4 weeks, female) (*b*), and weight assessment (*c*) of CON and *Ezh2* cKO^{osx} animals. *d–f*, μCT analysis of skulls (*d* and *e*) and clavicles (*f*) of CON and *Ezh2* cKO^{osx} animals (3 weeks, male). *Error bars*, S.E.

growth plate and cartilage formation, *Ezh2* loss leads to increased bone marrow adiposity and yields a mild low trabecular bone phenotype in young animals. The latter finding indicates that *Ezh2* function in osteoblasts is required for formation or maintenance of trabecular bone.

Cre-specific recombination of the Ezh2 conditional allele results in the loss of EZH2 protein in primary calvarial osteoblasts

The SET domain of EZH2 possesses H3K27 methyltransferase activity, and its loss renders EZH2 inactive. To assess the efficiency of the Cre-recombination of the *Ezh2* conditional allele (42) in osteoblasts, primary calvarial osteoblasts derived from *Ezh2*$^{flox/flox}$ were infected with adenovirus expressing GFP (Ad-GFP) or an adenovirus expressing GFP and Cre recombinase (Ad-GFP-Cre) (Fig. 4*a*). The administration of Ad-GFP to these cells is expected to generate WT *Ezh2*, whereas the addition of Ad-GFP-Cre is predicted to result in truncated *Ezh2* lacking the SET domain (Fig. 4*b*). As anticipated, administration of both adenoviruses results in the expression of GFP, whereas Cre recombinase expression is only detected in the cells infected with Ad-GFP-Cre (Fig. 4*c*). To detect the mutant *Ezh2* allele, a primer pair that spans across exons 15 and 20 was used (Fig. 4*b*). The addition of Ad-GFP does not induce gene rearrangement, but the addition of Ad-GFP-Cre results in the formation of the mutant *Ezh2* allele (Fig. 4*c*). Furthermore, we observe a reduction in the expression of the SET domain and total *Ezh2* mRNA levels. The addition of Ad-GFP-Cre results in the loss of EZH2 protein levels as detected by Western blotting 4 days after infection (Fig. 4*d*). Collectively, these results demonstrate that Cre-specific recombination of the *Ezh2* locus results in fusion of exons 15 and 20 at the mRNA level and the loss of EZH2 protein in primary osteoblasts.

Loss of functional Ezh2 inhibits osteoblast differentiation of bone marrow–derived mesenchymal stem cells

To assess a direct effect of *Ezh2* loss on progenitor cells, BMSCs were isolated from 6–8-week-old male and female CON and *Ezh2* cKO^{Osx} mice and differentiated into the osteogenic lineage (Fig. 5). RT-qPCR analysis demonstrates that expression of osteogenic genes (*e.g.* osterix/*Sp7*, osteocalcin/

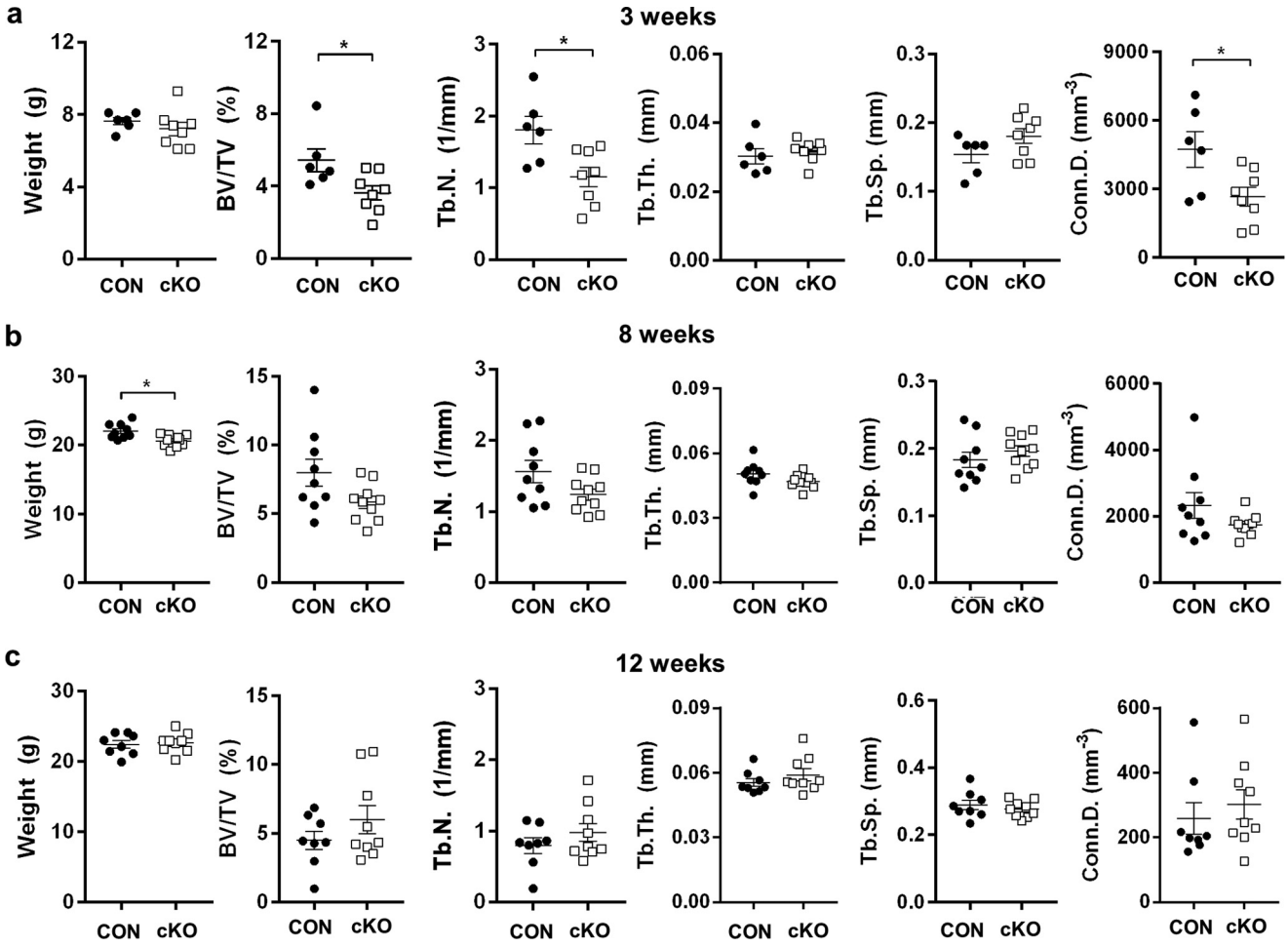

Figure 2. Osteoblastic loss of *Ezh2* induces a low trabecular mass phenotype in young animals. *a–c*, weights of animals assessed as well as tibial trabecular bone parameters assessed by μCT of CON and *Ezh2* cKO^{Osx} male mice at 3 (*a*), 8 (*b*), and 12 (*c*) weeks of age. Structural parameters measured by μCT include trabecular bone volume fraction (*BV/TV*, %), trabecular number (*Tb.N.*, mm^{-1}), trabecular thickness (*Tb.Th.*, mm), trabecular separation (*Tb.Sp*, mm), and connectivity density (*ConnD*, 1/mm^3). *Error bars*, S.E.

Bglap, alkaline phosphatase/*Alpl*, and bone sialoprotein/*Ibsp*) is suppressed in male and female *Ezh2* cKO^{Osx} BMSCs undergoing osteogenic differentiation (Fig. 5*a*). In support of RT-qPCR analysis, alizarin red staining of BMSCs cultures on day 17 of osteogenic differentiation demonstrates a significant reduction in mineral deposition with *Ezh2* loss (Fig. 5, *b* and *c*). Similar to alizarin red staining, a reduction in alkaline phosphatase staining is observed with BMSCs derived from *Ezh2* cKO^{osx} animals (Fig. S2). Western blot analysis reveals that EZH2 expression is reduced, whereas H3K27me3 is increased during osteogenic commitment of mouse-derived BMSCs (Fig. 5*d*). A reduction in EZH2 and H3K27me3 is observed (see days 3 and 7) in BMSCs derived from *Ezh2* cKO^{osx} animals. As a loading control, the levels of histone H3 remain stable during the differentiation time course. Hoechst staining, which is a proxy for the number of cells in each treatment condition, reveals that *Ezh2* loss results in the reduction of DNA content at day 7 (Fig. 5*e*). These results show that *Ezh2* is only actively expressed during early proliferative stages of BMSC differentiation and that H3K27me3 levels are controlled by another enzyme (*e.g.* EZH1) at later maturation stages of osteogenic differentiation in BMSCs. Furthermore, the loss of osteogenic potential of BMSCs upon genetic *Ezh2* loss demonstrates that *Ezh2* performs a critical and previously unrecognized positive function during proliferative expansion of BMSCs as they gradually become committed to Osx-positive osteoprogenitor cells within the population.

It is plausible that loss of *Ezh2* in Osx-positive osteoblasts *in vivo* may affect regulatory interplay with BMSCs *in situ* within the bone environment. Hence, the BMSCs isolated from *Osx-Cre*–positive mice may differ from naive BMSCs developing in the bone micro-niche of WT mice. Therefore, we assessed BMSCs differentiation after acute deletion of *Ezh2 in vitro* utilizing Ad-GFP and Ad-GFP-Cre virus particles on BMSCs from *Ezh2*$^{flox/flox}$ animals that are otherwise genetically and phenotypically normal (Fig. 6*a*). Corroborating our data obtained with primary calvarial osteoblasts (Fig. 4), the addition of Ad-GFP-Cre resulted in the expression of Cre recombinase and the truncated version of *Ezh2* (*Ezh2*^{mut}) (Fig. 6*b*). In addition, a reduction in WT mRNAs that encompass the *Ezh2* SET domain (*Ezh2*^{SET}) and total *Ezh2* mRNA is observed. Acute loss of *Ezh2* results in a small, but significant, reduction in cell viability as measured by MTS activity 10 days after the addition of virus particles (Fig. 6*c*). Although not significant, DNA content as measured by Hoechst staining is also reduced as a result of *Ezh2* loss in BMSCs (Fig. 6*d*). Acute deletion of *Ezh2* reduces

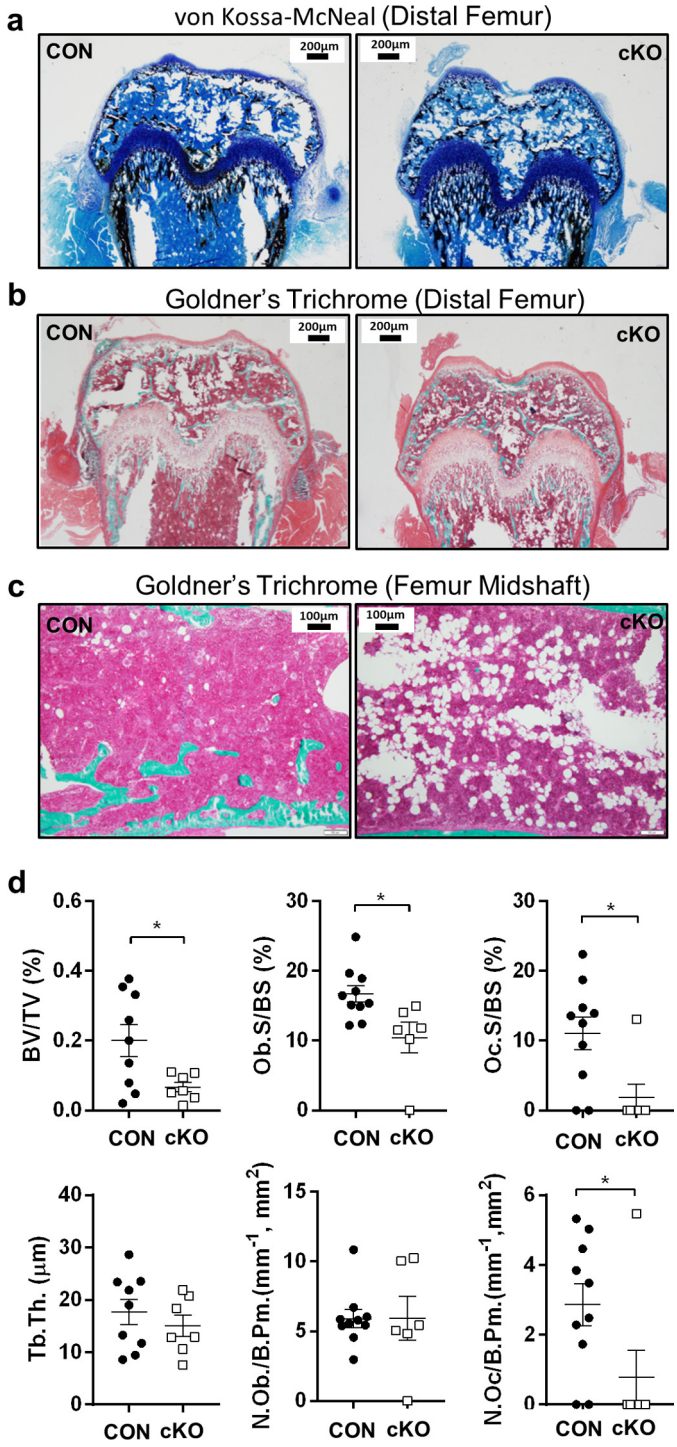

Figure 3. Osteoblast-specific loss of *Ezh2* results in osteoblast and osteoclast alterations in young mice. *a* and *b*, Von Kossa–McNeal (*a*) and Goldner's trichrome (*b*) staining of distal femurs (3 week old, male). *c*, Goldner's trichrome staining of femur mid-shafts (3 weeks old, male). *d*, static histomorphometry analysis of femurs derived from 3-week-old male CON and *Ezh2* cKO^{Osx} animals. Histomorphometric parameters measured include trabecular bone volume fraction (*BV/TV*, %), osteoblast surface (*Ob.S/BS*, %), osteoclast surface (*Oc.S/BS*, %), trabecular thickness (*Tb.Th*, μm), number of osteoblasts per bone perimeter (*N.Ob./B.Pm.*, mm^{-1}, mm^2), and number of osteoclasts per bone perimeter (*N.Oc./B.Pm.*, mm^{-1}, mm^2). *Error bars*, S.E.

the expression of several osteogenic markers (*e.g. Bglap*, *Ibsp*, *Alpl*, and osteomodulin/*Omd*) at day 14 after osteogenic induction (Fig. 6*e*). In support of mRNA reduction of key osteogenic genes, a significant reduction in alizarin red staining of these primary cell cultures is observed (Fig. 6, *f* and *g*). Western blot analysis demonstrates a loss of EZH2 protein and a reduction in H3K27me3 with the addition of Ad-GFP-Cre (Fig. 6*h*). Consistent with the loss of the exon encoding the SET domain upon Cre excision, a faster migrating EZH2 protein band is observed after the recombination event, reflecting the truncated short-lived residual EZH2 protein that lacks methyl transferase activity. Taken together, our data show that EZH2 protein expression is lost during both *in vivo* excision (*Ezh2* cKO^{Osx}) and *ex vivo* excision of *Ezh2* (Ad-GFP-Cre with Ezh2$^{flox/flox}$ BMSCs). Our results indicate that loss of EZH2 protein reduces cellular H3K27me3 levels, which in principle is permissive for osteogenic differentiation but may simultaneously inhibit osteogenic differentiation of primary mouse BMSC populations by reducing the number of osteogenic progenitor cells. This finding corroborates the emerging idea that *Ezh2* performs an essential cellular function during osteoprogenitor proliferation while suppressing the bone cell maturation program.

Acute loss of Ezh2 impacts cell cycle progression in mouse BMSCs

Because loss of *Ezh2* reduces cell number (as assessed by DNA content) and metabolic activity (as monitored by MTS assays), we examined the contribution of *Ezh2* to cell cycle progression of BMSCs derived from WT (C57/BL6) or *Ezh2*$^{flox/flox}$ mice (Fig. 7*a*). The infection of these BMSCs with Ad-GFP-Cre virus results in expression of GFP in both female and male BMSCs (Fig. 7*b*), which results in the expected recombination of *Ezh2* locus in *Ezh2*$^{flox/flox}$ BMSCs (data not shown). RT-qPCR analysis shows stable expression of the housekeeping gene eukaryotic elongation factor 1α1 (*Eef1a1*) when normalized to that of the housekeeping gene *Gapdh* at day 6 after infection (Fig. 7*c*). However, loss of *Ezh2* suppresses the expression of two proliferation markers, *Mki67* and *Ccnb2*, that encode the Ki67 antigen and cyclin B2, respectively. Furthermore, the two principal mRNA products (p16 and p19) of the *Cdkn2a* locus, which are critical inhibitors of cell cycle progression, are significantly up-regulated with *Ezh2* loss. A similar trend is also observed with *Cdkn1a* (p21), another cell cycle inhibitor. Flow cytometric analysis shows that loss of *Ezh2* alters the distribution of cells in the different phases of the cell cycle (Fig. 7*d*). In both male and female BMSCs, the loss of *Ezh2* significantly shifts the cells from S/G_2 phases into the G_0/G_1 phases of the cell cycle, suggesting that cell cycle progression of BMSCs is impeded in the G_0 or G_1 phase when EZH2 activity is eliminated. Because male and female cells were processed independently, these technical considerations limit direct comparison of cell cycle distributions between the two sexes. In support of these findings, MTS activity assays show reduced metabolic activity on days 6 and 11 with *Ezh2* loss (Fig. 7*e*). No significant changes are observed day after plating (day 0) and 3 days after the addition of the virus to the cell populations. Thus, *Ezh2* loss in BMSCs reduces the number of cells by attenuating G_0 or G_1 cell cycle progression in BMSCs.

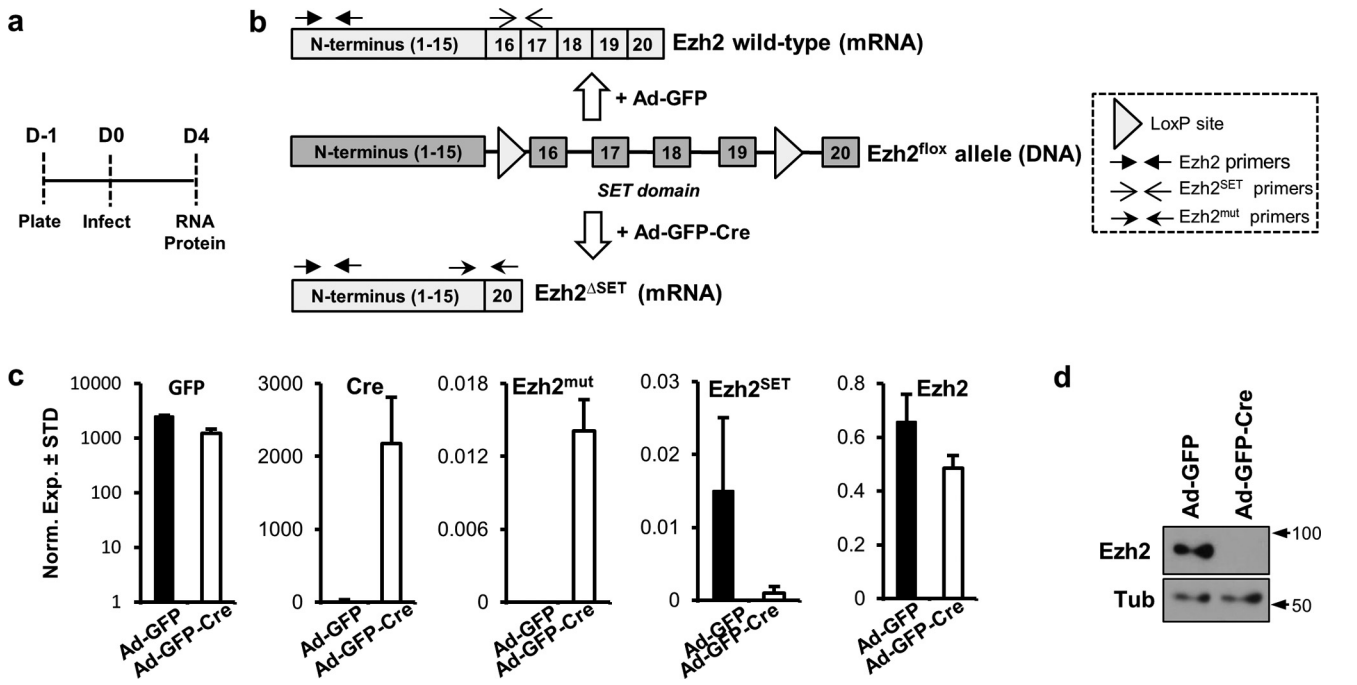

Figure 4. Cre expression in *Ezh2*$^{flox/flox}$ calvarial osteoblasts results in the loss of EZH2 protein. *a*, illustration of the experimental protocol for Ad-GFP/Ad-GFP-Cre infection of primary calvarial osteoblasts derived from 2–3-day-old *Ezh2*$^{flox/flox}$ animals. *b*, schematic diagram of the *Ezh2*$^{flox/flox}$ allele, showing the recombination event and highlighting the use RT-qPCR primers to detect WT, mutated (truncated), and SET domain of *Ezh2*. *c*, expression of GFP, Cre, *Ezh2*^{mut}, *Ezh2*^{SET}, and total *Ezh2* mRNA levels 4 days after the addition of Ad-GFP and Ad-GFP-Cre ($n = 3$). *d*, Western blot analysis 4 days after the infection of cells. *Error bars*, S.D.

Altered expression of cell cycle genes in mouse calvaria lacking Ezh2 expression

To investigate the mechanism by which *Ezh2* controls cell cycle progression, we examined *in vivo* gene expression by RNA-Seq analysis of mRNAs derived from calvaria of CON and *Ezh2* cKO pups (Fig. 8). Consistent with genomic truncation of the *Ezh2* locus through Cre excision over *loxP* sites, RNA-Seq analysis of mRNA collected from *Ezh2* cKO calvaria exhibits a marked reduction in the number of reads mapped to exons 16–19 (Fig. 8, *a* and *b*). Bio-informatic analysis of genes with robust average expression (>0.1 reads/kilobase pair/million mapped reads (RPKM)) demonstrates that ~500 genes are up-regulated and ~200 genes are down-regulated upon loss of *Ezh2* (fold change > 1.4 and p value < 0.05) (Fig. 8*c*). Similar to observations in primary BMSC cultures, the cell cycle–inhibitory gene *Cdkn2a* is one of the most prominently up-regulated genes in *Ezh2* cKO calvaria (Fig. 8, *c* and *d*). Of the ~700 differentially expressed genes, about 8.5% ($n = 61$) associate with the gene ontology biological process term "cell cycle" (Fig. 8*e*). These RNA-Seq results corroborate findings obtained with *ex vivo* cultures of BMSCs and establish that genetic loss of *Ezh2* perturbs *in vivo* expression of cell cycle–regulatory genes in mouse calvaria.

Discussion

Our group has pursued multiple strategies for understanding the cell-autonomous effects of *Ezh2* in mesenchymal stromal cells and committed osteoblasts within bone tissue (reviewed in Ref. 18). We have previously shown that genetic inactivation of *Ezh2* in calvarial bones (*Ezh2* cKO^{Prrx1}, *Ezh2*$^{flox/flox}$*:Prrx1-Cre*) enhances expression of osteogenic genes. These mice exhibited several major phenotypic changes, including a domed head and premature suture fusion (*i.e.* craniosynostosis) (26), a phenotype that could originate from any development stage when the *Prrx1* promoter first begins to express Cre. This permanent genetic deletion of *Ezh2* at an early developmental stage limited our interpretation. However, these studies did not permit a direct assessment of the acute cell-autonomous mechanistic effects of *Ezh2* deletion in osteoblasts during normal skeletal patterning. Our present study assessed the genetic role of *Ezh2* in the osteoblastic lineage and demonstrates that *Ezh2* is necessary for early proliferative stages of osteoblastogenesis. This function complements its known activity as a suppressor of osteoblast maturation.

Conditional deletion of *Ezh2* in osteoblasts *in vivo* (using the Osx/Cre driver) results in mice with normal skeletal patterning. Female animals do not exhibit any obvious anatomical changes, whereas male cKO mice weigh less than CON animals at 3 and 8 weeks of age. μCT reconstructions indicate that skull structure, calvaria suture formation, and clavicle formation are within the normal range of variation in mice lacking *Ezh2* in the osteoblast lineage. Interestingly, μCT analysis reveals a mild low trabecular bone mass phenotype at 3 weeks of age that resolves at 8 weeks. These findings are supported by histomorphometric analysis at 3 weeks of age. Interestingly, a reduction in osteoblasts is accompanied by a reduction in osteoclasts at 3 weeks of age, suggesting that bone formation and resorption remain coupled with osteoblastic loss of *Ezh2*. This coupling effect is also observed at 12 weeks of age, where the number of osteoclasts is significantly different between control and *Ezh2* cKO animals. Histologic assessment reveals normal growth plate and cartilage development but shows enhanced formation

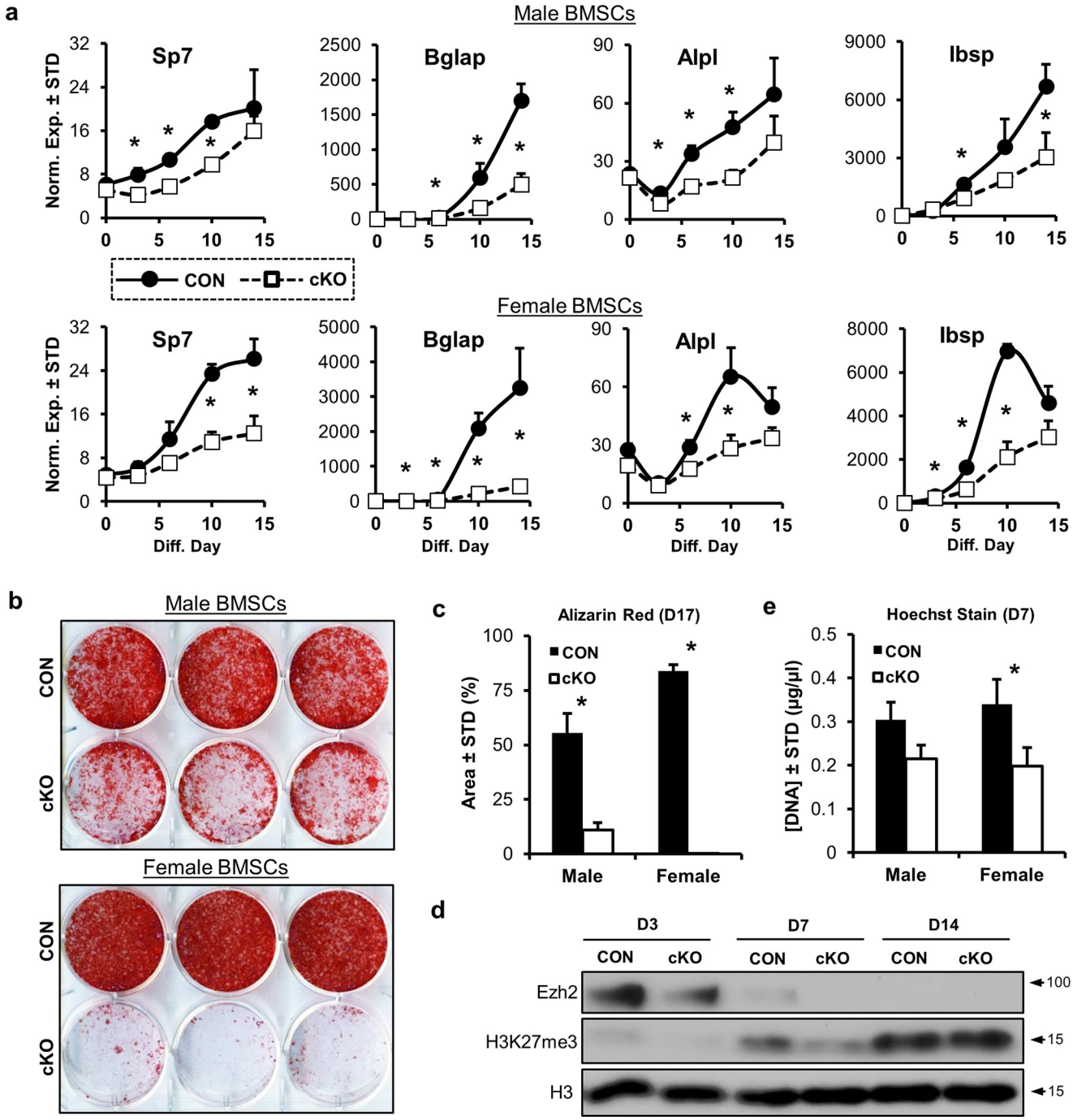

Figure 5. Genetic loss of *Ezh2* inhibits osteogenic differentiation of BMSCs. BMSCs were isolated from male and female 6–8-week-old CON and *Ezh2* cKO^{Osx} mice and differentiated into the osteogenic lineage as described under "Experimental procedures." *a*, RT-qPCR analysis of osteogenic markers during osteogenic commitment of BMSCs ($n = 3$). *b* and *c*, alizarin red staining (*b*) and quantification (*c*) of BMSCs differentiated for 17 days ($n = 3$). *d*, Western blot analysis of *Ezh2* and H3K27me3 levels in BMSCs (male) undergoing osteogenic differentiation. *e*, Hoechst staining (DNA content) of BMSCs differentiated for 7 days ($n = 3$). *Error bars*, S.D.

of cells positive for lipid droplets in the bone marrow cavity of cKO animals. Loss of *Ezh2* in mouse BMSCs reduces osteogenic differentiation *ex vivo*, in part because of negative effects on cell cycle progression that occur concomitant with up-regulation of cyclin-dependent kinase inhibitors (*e.g.* CDKN2A/p16^{INK4A}-p19^{ARF}) and down-regulation of genes supporting mitotic division (*e.g.* cyclin B2). Consistent with these results, changes in the expression of cell cycle genes are also observed in *Ezh2* cKO calvaria. Of interest, BMSCs from 6–8-week-old *Ezh2* cKO animals exhibit a reduction in osteogenic differentiation, but the bone parameters resolve at this age *in vivo*. This suggests that *Ezh2* is required for the commitment of progenitor cells into the osteogenic lineage, whereas coupling between osteoblast and osteoclast restores net trabecular bone formation *in vivo*. We note that the contribution of *Ezh2* to cell cycle progression has been well documented (43–45) for nonosseous cell types and that small-molecule inhibitors of EZH2 are used clinically to inhibit cancer cell proliferation (46, 47). Taken

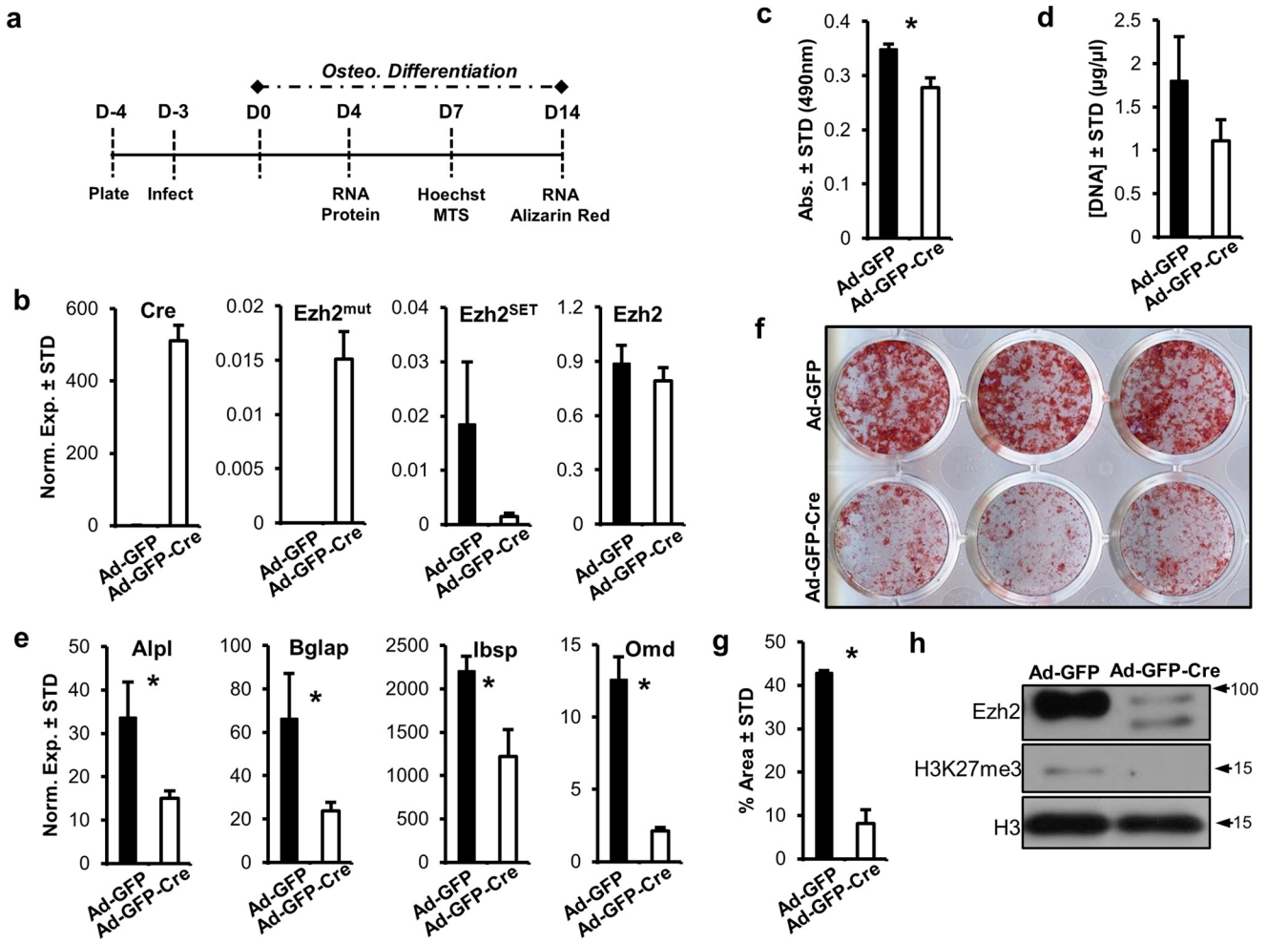

Figure 6. Acute loss of *Ezh2* inhibits osteogenic differentiation of BMSCs. *a*, BMSCs were isolated from 7-week-old *Ezh2*$^{flox/flox}$ male mice, infected with Ad-GFP or Ad-GFP-Cre, and differentiated into the osteogenic lineage. *b*, expression of Cre, *Ezh2*^{mut}, *Ezh2*^{SET}, and total *Ezh2* mRNA levels on day 4 of osteogenic differentiation ($n = 3$). *c* and *d*, MTS toxicity assay ($n = 3$) (*c*) and Hoechst staining (DNA content) ($n = 3$) (*d*) on day 7 of differentiation. *e*, RT-qPCR analysis of osteogenic markers on day 14 of differentiation ($n = 3$). *f* and *g*, alizarin red staining (*f*) and quantification ($n = 3$) (*g*) on day 14 of differentiation. *h*, Western blot analysis of EZH2 refers to protein and H3K27me3 on day 4 of osteogenic differentiation. *Error bars*, S.D.

together, our study indicates that *Ezh2* controls osteoblastic differentiation by both supporting cell cycle progression of osteoblast progenitor cells and suppressing maturation of precursor cells that are committed to the osteoblast lineage.

The gain in our understanding that *Ezh2* is a bifunctional regulator of osteoblastogenesis clarifies several other previous results. For example, previous studies have shown that mesenchymal loss of *Ezh2* results in several skeletal abnormalities (26, 37), and these apparent patterning defects can now be interpreted as resulting from a reduction in the expansion of committed osteoblast progenitors when *Ezh2* is inactivated in *Ezh2* cKO mice that express the Prrx1-Cre driver. The *in vivo* importance of *Ezh2* in osteoprogenitor cells during early stages of bone formation in skeletally immature mice is corroborated by our observation that *Ezh2* cKO that express the *Osx-Cre* driver have a transient low trabecular bone volume phenotype in young adult mice. Thus, genetic inactivation of *Ezh2* in early stages of skeletogenesis generally has negative biological effects. However, *Ezh2* inhibition also has clear bone-stimulatory potential from the perspectives of both bone tissue engineering and bone anabolic therapy. For example, transient loss of EZH2 function (knockdown or small-molecule inhibitors) in cultured mesenchymal cells stimulates osteogenic differentiation *in vitro*, and EZH2 inhibition also enhances *in vivo* bone formation and prevents bone loss associated with estrogen depletion (26, 28, 29, 33, 34).

Our previous work has indicated that *Ezh2* loss in the mesenchymal compartment yields a senescence-like phenotype, characterized by enhanced expression of *Cdkn2a*, a well-characterized cell cycle and senescence marker, as well as enhanced bone marrow lipid droplet formation (26). Deletion of *Ezh2* co-regulators, *Hdac3* and *Zfp521*, in osteoblast progenitors produces similar marrow phenotypes (48–50). Our current study also shows that *Ezh2* loss results in bone marrow adiposity and enhanced expression of *Cdkn2a*. It is plausible that the absence of *Ezh2* could potentially activate an adipogenic program that causes accumulation of fat droplets in cells that are precommitted to the osteogenic lineage. Indeed, fate-mapping studies have shown that *Osx-Cre*–positive cells can contain lipid droplets (51, 52). These data suggest that, similar to *Hdac3* (53), *Ezh2* could potentially regulate lipid storage in pre-osteoblasts. It is noteworthy that the expression of *Cdkn2a* is more

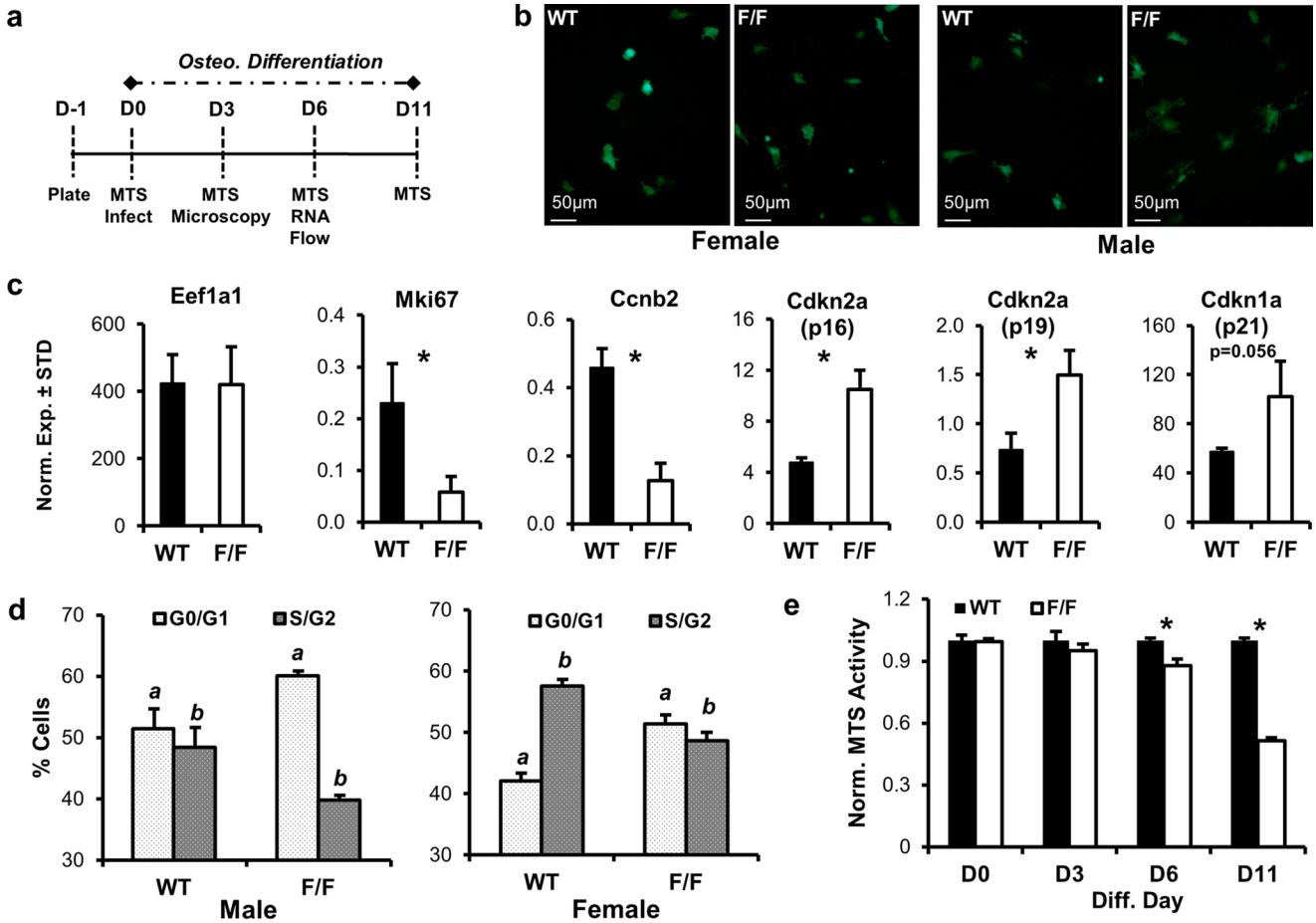

Figure 7. Acute loss of *Ezh2* disrupts the cell cycle in BMSCs. *a*, BMSCs were isolated from 6–8-week-old C57/B6 CON and *Ezh2*$^{flox/flox}$ male and female mice, infected with Ad-GFP-Cre, and differentiated into the osteogenic lineage. *b*, microscopy images on day 3 of GFP expression (*green*) in male and female BMSCs infected with Ad-GFP-Cre. *c*, RT-qPCR analysis (day 6) of *Eef1a1* and several cell cycle markers in BMSCs (male, $n = 3$). *d*, cell cycle analysis (day 6) of male and female BMSCs ($n = 3$). *Letters* (*a* and *b*) denote significance between *columns* within each of the two *panels*. *e*, MTS activity assay of BMSCs at various time points after infection and induction of differentiation (female, $n = 3$). *Error bars*, S.D.

robust in primary calvaria derived from animals that lack *Ezh2* expression in the mesenchyme (26) when compared with animals that lack expression of this epigenetic enzyme in pre-osteoblasts (current study). Our current and past findings are also supported by a recent study that shows that the loss of *Ezh2* in Nestin-expressing cells, a population of mesenchymal stem cells, induces a senescence phenotype in mice (54).

Recent studies have demonstrated that EZH2 possesses methyltransferase-independent function (55–57). Therefore, we considered that *Ezh2* inactivation by elimination of the SET domain in principle still could result in a truncated EZH2 protein that may retain some of its biochemical functions. We consider it less likely as this mutant protein is rapidly degraded in mesenchymal cells. Permanent *Ezh2* loss by genetic inactivation is expected to destabilize the PRC2 complex, resulting in weakening of chromatin structure and inducing gene expression changes indirectly. Long-term loss during development could potentially provoke compensatory mechanisms to ensure skeletal formation that proceeds through less efficient mechanisms.

Our group and others have previously presented solid data in support of the concept that *Ezh2* inhibition has bone-stimulatory properties (26, 28, 29, 33, 34). The present work indicates that inhibitory strategies could also provoke negative effects on bone, especially during initial stages of bone growth. Notwithstanding this limitation in these negative biological effects during maturation of the mammalian skeleton, it may still remain realistic to leverage EZH2 inhibition for short-term, local applications in skeletally mature mammalian species and in bone tissue engineering to accelerate maturation of committed osteoblasts. Therapeutic strategies utilizing EZH2 inhibitors could potentially be employed to enhance spinal fusion, stimulate orthopedic implant grafting, and heal nonunion fractures. However, EZH2 inhibition is clearly not beneficial for adolescent or young adult mice; nor does it appear to be suitable for long-term applications (*i.e.* chronic conditions such as osteoporosis). Our current data indicate that undesired effects of EZH2 suppression, including cell cycle impediment and senescence, may counter the beneficial effects (*i.e.* enhanced expression of osteogenic genes) in bone-stimulatory strategies.

Experimental procedures

Calvarial osteoblast culture

Calvaria (parietal and frontal bones) were dissected from 2–3-day-old *Ezh2*$^{flox/flox}$ pups and digested three times (20 min,

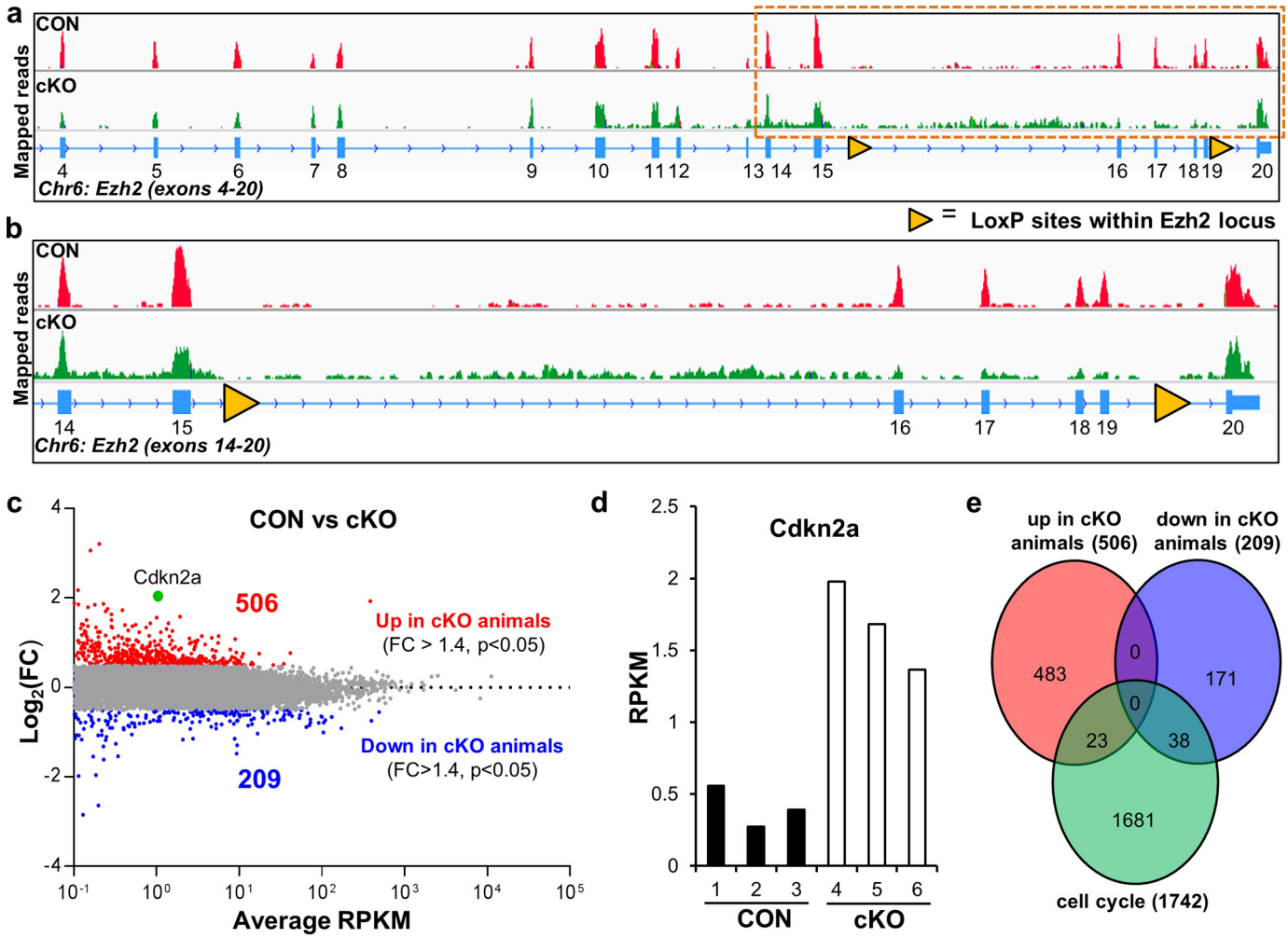

Figure 8. Changes in expression of cell cycle genes with *Ezh2* loss in mouse calvaria. Calvaria were isolated from 2–3-day-old CON and Ezh2 cKO female pups, and RNA-Seq analysis was performed ($n = 3$). *a*, genome browser view (IGV) of *Ezh2* exons 4–20. Exons 1–3 were omitted due to space constraints (a very long intron between exons 3 and 4). *b*, a closer IGV view of exons 14–20. The SET domain is located within exons 16–19 of *Ezh2*. *c*, gene expression changes with the loss of *Ezh2* in mouse calvaria based on -fold change (*FC*) > 1.4 and *p* value < 0.05. All genes with an average expression > 0.1 RPKM were included in the analysis. Significantly up-regulated (*red*, $n = 506$) and down-regulated (*blue*, $n = 209$) genes are *highlighted*. Expression of *Cdkn2a* in CON and cKO calvaria (*d*). *e*, Venn diagram analysis showing that cell cycle–related genes exhibit altered expression with the loss of *Ezh2* in calvaria.

1 h, and 1 h) in collagenase digestion medium (αMEM, 2 mg/ml collagenase type II, and 0.005% trypsin) at 37 °C (58). The cells from the third digest and the remaining calvarial bones were plated and maintained in αMEM supplemented with 10% FBS, 1% antibiotic and antimycotic, and 1% nonessential amino acids. Passage 2 cells were plated (16,000 cells/cm^2) and infected with Ad-GFP or Ad-GFP-Cre (Vector Biolabs).

Bone marrow mesenchymal stem cell cultures

BMSCs were isolated from WT C57Bl/6 mice, *Ezh2*$^{flox/flox}$ animals, or *Ezh2* CON or *Ezh2* cKO^{Osx} mice, as described (59). Briefly, bone marrow was flushed from femurs and tibias of 6–8-week-old mice, which is an age that yields a robust and consistent number of BMSCs. Cells were immediately seeded for experiments in 6- and 12-well plates (1 million cells/cm^2) or cultured in T175 flasks for 4–6 days before seeding the adherent cell population in 6- and 12-well plates (20,000 cells/cm^2). BMSCs were maintained in αMEM supplemented with 20% FBS, 1% antibiotic and antimycotic, and 1% nonessential amino acids. BMSCs were selected by their ability to adhere to the culture plates (at least 3 days) before exposure to adenovirus and differentiation medium. Osteogenic differentiation was accomplished by the addition of 50 μg/ml ascorbic acid, 10 mM β-glycerol phosphate, and 10^{-8} M dexamethasone in the maintenance medium. Media were changed every 3 days.

MTS activity assay

MTS activity was assayed according to the manufacturer's protocol (Promega). Absorbance was measured at 490 nm using a SpectraMAX Plus spectrophotometer (Molecular Devices).

Hoechst staining

Medium was aspirated from wells, and cells were washed one time with PBS. After aspiration of PBS, 500 μl of Hoechst 33258 (Sigma, 94403) (0.5 μl/ml in PBS) was added to each well. Plates were left to incubate in the dark at room temperature for 20 min. After incubation, fluorescence intensity was measured at a 340-nm excitation wavelength and 460-nm emission wavelength using an F200 Infinite Pro (Tecan) plate reader. Meas-

urements were fit to a standard DNA curve to determine relative DNA content.

RT-qPCR

RNA was isolated using the Direct-zol™ RNA kit (Zymo Research). RNA was then reverse-transcribed into cDNA by the SuperScript III first-strand synthesis system (Invitrogen). Transcript levels were measured using the $2^{\Delta\Delta Ct}$ method and normalized to the housekeeping gene *Gapdh* (set at 100). Gene-specific primers are shown (Table S3).

Western blotting

Cell lysis and Western blotting were performed as described previously (26, 29). Proteins were visualized using the ECL Prime detection kit. Primary antibodies used were as follows: actin (1:10,000; sc-1616, Santa Cruz), H3 (1:10,000; 05-928, Millipore), H3K27me3 (1:5,000; 17-622, Millipore), EZH2 (1:10,000; 5246, Cell Signaling), and tubulin (1:10,000; E7, University of Iowa Hybridoma Bank).

Alkaline phosphatase and alizarin red staining

For alkaline phosphatase activity, cell cultures were fixed in 10% neutral buffered formalin and stained with 5-bromo-4-chloro-3-indolyl-phosphate/nitro blue tetrazolium to monitor the enzymatic activity of alkaline phosphatase (Promega). For alizarin red staining, cells were also fixed in 10% neutral buffered formalin and stained with 2% alizarin red to visualize calcium deposition. Absorption of alizarin red stain was quantified with ImageJ software (60).

Animal welfare

Animal studies were conducted according to guidelines provided by the National Institutes of Health and the Institute of Laboratory Animal Resources, National Research Council. The Mayo Clinic Institutional Animal Care and Use Committee approved all animal studies. Animals were housed in an accredited facility under a 12-h light/dark cycle and provided water and food (PicoLab Rodent Diet 20, LabDiet) *ad libitum*.

Deletion of function Ezh2 in osteoblasts

Mice containing a conditional *Ezh2*$^{fl/fl}$ allele (42) flanking the SET domain were obtained from a Mutant Mouse Regional Resource Center (B6;129P2-*Ezh2*tm1Tara/Mmnc, University of North Carolina, Chapel Hill, NC). *Ezh2* function was conditionally deleted in osteoblasts by these mice with animals that express Cre recombinase under the control of the *Sp7*/*Osx* promoter (41). Our studies characterized CON (*Ezh2*$^{wt/wt}$*: Osx-Cre*$^{+}$) and conditional knockout (*Ezh2* cKO^{osx}, *Ezh2*$^{flox/flox}$*: Osx-Cre*$^{+}$) animals. The following primers were used for genotyping: *Ezh2* (forward, TGTCATGTCTGGGTCTAATGCTAC; reverse, GGAACCTCGCTATGTGTAACCA) and *Cre* (forward, TCCAATTTACTGACCGTACACCAA; reverse, CCTGATCCTGGCAATTTCGGCTA).

Micro-computed tomography analysis

Right tibias were harvested from 3-, 8-, and 12-week–old CON and *Ezh2* cKO^{osx} mice. Soft tissue surrounding the bone was carefully removed, and samples were fixed in 10% neutral buffered formalin for 48 h followed by storage in 70% ethanol. Tibias were scanned with an *ex vivo* μCT system (Skyscan 1174, Skyscan) equipped with a 50-kV, 800-μA X-ray tube and a 1.3-megapixel charge-coupled device coupled to a scintillator. Samples were maintained in a moist environment during scanning to prevent dehydration and scanned in air using 8-μm (3 and 8 weeks old) or 10-μm (12 weeks old) isotropic voxels with an integration time of 400 ms. The region of analysis selected was between 13 and 16% of bone length (3-week-old mice) or between 12 and 15% of bone length (8- and 12-week-old mice) relative to the proximal tibial epiphysis for trabecular bone analysis. Mid-shafts of the tibias were assessed for the cortical parameters. Reconstructions were performed in NRecon software (Skyscan) and subjected to morphometric analyses using CTAn software (Skyscan). A minimum gray scale threshold of 60 (3 weeks old) or 70 (8 and 12 weeks old) was used.

Skulls were harvested from 3-week-old CON and *Ezh2* cKO^{osx} mice. Samples were fixed in 10% neutral buffered formalin for 48 h followed by storage in 70% ethanol. Skulls were scanned using a Scanco vivaCT40 system (Scanco) at 70 kV, 114 μA with an integration time of 221 ms for a 10.5 isometric voxel size. 3D renderings were created using Microview (Parallax).

Histology and histomorphometric analysis

Right femurs were harvested from 3- and 12-week– old CON and *Ezh2* cKO^{osx} animals. Soft tissue surrounding the bone was carefully removed, and samples were fixed in 10% neutral buffered formalin for 48 h followed by storage in 70% ethanol. Undecalcified femurs were embedded in methyl methacrylate resin and sectioned using a rotary retracting microtome. Sections of 5-μm thickness were stained by Gomori's trichrome method as described previously (61). Calcified bone was visualized in green and osteoid in red. Quantitative histomorphometry was performed utilizing OsteoMeasure™ to estimate the percentage of bone volume (BV/TV, %), osteoblast surface, osteoid surface, and number of osteoblasts and osteoclasts per bone parameter. In addition, trabecular thickness (μm) was also derived from trabecular parameters. Six fields of view were measured, scanning a total area of 2.1 mm^2 at a distance of ~1 mm away from the growth plate. All measurements were made in the trabecular region. Cortical bone was marked as nontissue and was not included in the measurements.

Flow cytometric analysis

Cells were harvested by trypsin, washed with PBS, and fixed in 70% ethanol overnight at 4 °C. Cells were then washed two times with PBS and stained with 0.5 ml of FxCycle propidium iodide/RNase staining solution (Molecular Probes) for 30 min at room temperature in the dark. Cell cycle distribution (>10,000 events) was collected on the FACSCanto system (BD Biosciences), and the data were analyzed utilizing FACSDiva version 8.0.1 software (BD Biosciences).

High-throughput RNA sequencing and bioinformatic analysis of primary calvaria

Calvaria were dissected out from 2–3-day-old pups, washed in PBS, digested for 20 min in collagenase digestion medium (αMEM, 2 mg/ml collagenase type II, and 0.005% trypsin) at

37 °C, washed in PBS, and snap-frozen with liquid nitrogen and stored at −80 °C. RNA was then isolated utilizing Ultra Turrax T25 (IKA) and the Direct-zol™ RNA kit (Zymo Research). High-throughput read mapping and bioinformatic analyses for RNA-Seq were performed as reported previously (26, 27, 29, 62). Gene expression is expressed in RPKM. RNA-Seq data were deposited in the Gene Expression Omnibus of the National Institute for Biotechnology Information (GSE111245). Gene tracks were viewed using Interactive Genome Viewer (IGV) version 2.3.98 with the mm9 build loaded (63, 64). Cell cycle–related genes ($n = 1742$) have been obtained from the gene ontology consortium (65, 66).

Ex vivo assays

For assays that utilized primary calvarial osteoblasts and BMSCs, cells from several animals (typically 2–5) were pooled and then plated out as three biological replicates. These assays were repeated at least three times. Representative experiments are shown.

Statistics

For *ex vivo* studies, data are shown as mean ± S.D., and statistical analysis was performed with unpaired Student's *t* test. For *in vivo* studies, results are depicted by scatter plots that contain mean ± S.E. with each *dot* representing one mouse. To assess for bone parameters (μCT and histomorphometry), 6–10 animals derived from at least three independent litters were used in these studies. Statistical analysis was performed using Student's unpaired *t* test or Tukey post hoc tests for multiple comparisons using GraphPad Prism version 7 software. Significance is noted in the figures, when applicable (*, $p < 0.05$).

Author contributions—A. D. and A. J. v. W. designed the study. A. D., E. T. C., C. R. P., R. M. S., M. G., C. A. P., D. L. B., F. K., O. P., F. S. A., and R. E. performed the biological experiments. A. D., M. E., M. E. M. L., M. K., S. M. R., R. T., J. J. W., and A. J. v. W. provided interpretation of results and guidance of studies. A. D. and A. J. v. W. wrote the paper with comments from all authors.

Acknowledgments—We thank current and past members of our laboratory, including Eric Lewallen, Janet Denbeigh, Pengfei Zan, and Bashar Hasan, for stimulating discussions. We acknowledge the support of Asha Nair from the Bioinformatics Core, Medical Genome Facility, Microscopy and Cell Analysis Core, and Biomaterials Characterization and Quantitative Histomorphometry Core Facility.

References

1. Allis, C. D., and Jenuwein, T. (2016) The molecular hallmarks of epigenetic control. *Nat. Rev. Genet.* **17,** 487–500 CrossRef Medline
2. Gordon, J. A. R., Stein, J. L., Westendorf, J. J., and van Wijnen, A. J. (2015) Chromatin modifiers and histone modifications in bone formation, regeneration, and therapeutic intervention for bone-related disease. *Bone* **81,** 739–745 CrossRef Medline
3. Margueron, R., and Reinberg, D. (2011) The Polycomb complex PRC2 and its mark in life. *Nature* **469,** 343–349 CrossRef Medline
4. Margueron, R., Li, G., Sarma, K., Blais, A., Zavadil, J., Woodcock, C. L., Dynlacht, B. D., and Reinberg, D. (2008) Ezh1 and Ezh2 maintain repressive chromatin through different mechanisms. *Mol. Cell* **32,** 503–518 CrossRef Medline
5. Marchesi, I., Giordano, A., and Bagella, L. (2014) Roles of enhancer of zeste homolog 2: from skeletal muscle differentiation to rhabdomyosarcoma carcinogenesis. *Cell Cycle* **13,** 516–527 CrossRef Medline
6. Ge, K. (2012) Epigenetic regulation of adipogenesis by histone methylation. *Biochim. Biophys. Acta* **1819,** 727–732 CrossRef Medline
7. Montecino, M., Pockwinse, S., Lian, J., Stein, G., and Stein, J. (1994) DNase I hypersensitive sites in promoter elements associated with basal and vitamin D dependent transcription of the bone-specific osteocalcin gene. *Biochemistry* **33,** 348–353 CrossRef Medline
8. Stein, G. S., Lian, J. B., Stein, J. L., Van Wijnen, A. J., and Montecino, M. (1996) Transcriptional control of osteoblast growth and differentiation. *Physiol. Rev.* **76,** 593–629 CrossRef Medline
9. Montecino, M., Lian, J., Stein, G., and Stein, J. (1996) Changes in chromatin structure support constitutive and developmentally regulated transcription of the bone-specific osteocalcin gene in osteoblastic cells. *Biochemistry* **35,** 5093–5102 CrossRef Medline
10. Montecino, M., Frenkel, B., van Wijnen, A. J., Lian, J. B., Stein, G. S., and Stein, J. L. (1999) Chromatin hyperacetylation abrogates vitamin D-mediated transcriptional upregulation of the tissue-specific osteocalcin gene *in vivo*. *Biochemistry* **38,** 1338–1345 CrossRef Medline
11. Shen, J., Hovhannisyan, H., Lian, J. B., Montecino, M. A., Stein, G. S., Stein, J. L., and Van Wijnen, A. J. (2003) Transcriptional induction of the osteocalcin gene during osteoblast differentiation involves acetylation of histones h3 and h4. *Mol. Endocrinol.* **17,** 743–756 CrossRef Medline
12. Stein, G. S., van Wijnen, A. J., Imbalzano, A. N., Montecino, M., Zaidi, S. K., Lian, J. B., Nickerson, J. A., and Stein, J. L. (2010) Architectural genetic and epigenetic control of regulatory networks: compartmentalizing machinery for transcription and chromatin remodeling in nuclear microenvironments. *Crit. Rev. Eukaryot. Gene Expr.* **20,** 149–155 CrossRef Medline
13. Pike, J. W., Meyer, M. B., St John, H. C., and Benkusky, N. A. (2015) Epigenetic histone modifications and master regulators as determinants of context dependent nuclear receptor activity in bone cells. *Bone* **81,** 757–764 CrossRef Medline
14. Dudakovic, A., Evans, J. M., Li, Y., Middha, S., McGee-Lawrence, M. E., van Wijnen, A. J., and Westendorf, J. J. (2013) Histone deacetylase inhibition promotes osteoblast maturation by altering the histone H4 epigenome and reduces Akt phosphorylation. *J. Biol. Chem.* **288,** 28783–28791 CrossRef Medline
15. Håkelien, A. M., Bryne, J. C., Harstad, K. G., Lorenz, S., Paulsen, J., Sun, J., Mikkelsen, T. S., Myklebost, O., and Meza-Zepeda, L. A. (2014) The regulatory landscape of osteogenic differentiation. *Stem Cells* **32,** 2780–2793 CrossRef Medline
16. Meyer, M. B., Benkusky, N. A., Sen, B., Rubin, J., and Pike, J. W. (2016) Epigenetic plasticity drives adipogenic and osteogenic differentiation of marrow-derived mesenchymal stem cells. *J. Biol. Chem.* **291,** 17829–17847 CrossRef Medline
17. Wu, H., Gordon, J. A., Whitfield, T. W., Tai, P. W., van Wijnen, A. J., Stein, J. L., Stein, G. S., and Lian, J. B. (2017) Chromatin dynamics regulate mesenchymal stem cell lineage specification and differentiation to osteogenesis. *Biochim. Biophys. Acta* **1860,** 438–449 CrossRef Medline
18. Dudakovic, A., and van Wijnen, A. J. (2017) Epigenetic control of osteoblast differentiation by enhancer of zeste homolog 2 (EZH2). *Curr. Mol. Biol. Rep.* **3,** 94–106 CrossRef
19. Thaler, R., Maurizi, A., Roschger, P., Sturmlechner, I., Khani, F., Spitzer, S., Rumpler, M., Zwerina, J., Karlic, H., Dudakovic, A., Klaushofer, K., Teti, A., Rucci, N., Varga, F., and van Wijnen, A. J. (2016) Anabolic and antiresorptive modulation of bone homeostasis by the epigenetic modulator sulforaphane, a naturally occurring isothiocyanate. *J. Biol. Chem.* **291,** 6754–6771 CrossRef Medline
20. Khani, F., Thaler, R., Paradise, C. R., Deyle, D. R., Kruijthof-de Julio, M., Galindo, M., Gordon, J. A., Stein, G. S., Dudakovic, A., and van Wijnen, A. J. (2017) Histone H4 methyltransferase Suv420h2 maintains fidelity of osteoblast differentiation. *J. Cell Biochem.* **118,** 1262–1272 Medline
21. Sen, B., Uzer, G., Samsonraj, R. M., Xie, Z., McGrath, C., Styner, M., Dudakovic, A., van Wijnen, A. J., and Rubin, J. (2017) Intranuclear actin structure modulates mesenchymal stem cell differentiation. *Stem Cells* **35,** 1624–1635 CrossRef Medline

22. Samsonraj, R. M., Dudakovic, A., Manzar, B., Sen, B., Dietz, A. B., Cool, S. M., Rubin, J., and van Wijnen, A. J. (2018) Osteogenic stimulation of human adipose-derived mesenchymal stem cells using a fungal metabolite that suppresses the polycomb group protein EZH2. *Stem Cells Transl. Med.* **7,** 197–209 CrossRef Medline
23. Soreide, E., Denbeigh, J. M., Lewallen, E. A., Samsonraj, R. M., Berglund, L. J., Dudakovic, A., Cool, S. M., Nordsletten, L., Kakar, S., and van Wijnen, A. J. (2018) Fibrin glue mediated delivery of bone anabolic reagents to enhance healing of tendon to bone. *J. Cell Biochem.* **119,** 5715–5724 CrossRef Medline
24. Varela, N., Aranguiz, A., Lizama, C., Sepulveda, H., Antonelli, M., Thaler, R., Moreno, R. D., Montecino, M., Stein, G. S., van Wijnen, A. J., and Galindo, M. (2016) Mitotic inheritance of mRNA facilitates translational activation of the osteogenic-lineage commitment factor Runx2 in progeny of osteoblastic cells. *J. Cell Physiol.* **231,** 1001–1014 CrossRef Medline
25. van Wijnen, A. J., van de Peppel, J., van Leeuwen, J. P., Lian, J. B., Stein, G. S., Westendorf, J. J., Oursler, M. J., Im, H. J., Taipaleenmäki, H., Hesse, E., Riester, S., and Kakar, S. (2013) MicroRNA functions in osteogenesis and dysfunctions in osteoporosis. *Curr. Osteoporos. Rep.* **11,** 72–82 CrossRef Medline
26. Dudakovic, A., Camilleri, E. T., Xu, F., Riester, S. M., McGee-Lawrence, M. E., Bradley, E. W., Paradise, C. R., Lewallen, E. A., Thaler, R., Deyle, D. R., Larson, A. N., Lewallen, D. G., Dietz, A. B., Stein, G. S., Montecino, M. A., Westendorf, J. J., and van Wijnen, A. J. (2015) Epigenetic control of skeletal development by the histone methyltransferase Ezh2. *J. Biol. Chem.* **290,** 27604–27617 CrossRef Medline
27. Dudakovic, A., Gluscevic, M., Paradise, C. R., Dudakovic, H., Khani, F., Thaler, R., Ahmed, F. S., Li, X., Dietz, A. B., Stein, G. S., Montecino, M. A., Deyle, D. R., Westendorf, J. J., and van Wijnen, A. J. (2017) Profiling of human epigenetic regulators using a semi-automated real-time qPCR platform validated by next generation sequencing. *Gene* **609,** 28–37 CrossRef Medline
28. Hemming, S., Cakouros, D., Isenmann, S., Cooper, L., Menicanin, D., Zannettino, A., and Gronthos, S. (2014) EZH2 and KDM6A act as an epigenetic switch to regulate mesenchymal stem cell lineage specification. *Stem Cells* **32,** 802–815 CrossRef Medline
29. Dudakovic, A., Camilleri, E. T., Riester, S. M., Paradise, C. R., Gluscevic, M., O'Toole, T. M., Thaler, R., Evans, J. M., Yan, H., Subramaniam, M., Hawse, J. R., Stein, G. S., Montecino, M. A., McGee-Lawrence, M. E., Westendorf, J. J., and van Wijnen, A. J. (2016) Enhancer of Zeste homolog 2 inhibition stimulates bone formation and mitigates bone loss caused by ovariectomy in skeletally mature mice. *J. Biol. Chem.* **291,** 24594–24606 CrossRef Medline
30. Chen, Y. H., Yeh, F. L., Yeh, S. P., Ma, H. T., Hung, S. C., Hung, M. C., and Li, L. Y. (2011) Myocyte enhancer factor-2 interacting transcriptional repressor (MITR) is a switch that promotes osteogenesis and inhibits adipogenesis of mesenchymal stem cells by inactivating peroxisome proliferator-activated receptor γ-2. *J. Biol. Chem.* **286,** 10671–10680 CrossRef Medline
31. Chen, Y. H., Chung, C. C., Liu, Y. C., Yeh, S. P., Hsu, J. L., Hung, M. C., Su, H. L., and Li, L. Y. (2016) Enhancer of zeste homolog 2 and histone deacetylase 9c regulate age-dependent mesenchymal stem cell differentiation into osteoblasts and adipocytes. *Stem Cells* **34,** 2183–2193 CrossRef Medline
32. Wang, L., Jin, Q., Lee, J. E., Su, I. H., and Ge, K. (2010) Histone H3K27 methyltransferase Ezh2 represses Wnt genes to facilitate adipogenesis. *Proc. Natl. Acad. Sci. U.S.A.* **107,** 7317–7322 CrossRef Medline
33. Jing, H., Liao, L., An, Y., Su, X., Liu, S., Shuai, Y., Zhang, X., and Jin, Y. (2016) Suppression of EZH2 prevents the shift of osteoporotic MSC fate to adipocyte and enhances bone formation during osteoporosis. *Mol. Ther.* **24,** 217–229 CrossRef Medline
34. Fang, C., Qiao, Y., Mun, S. H., Lee, M. J., Murata, K., Bae, S., Zhao, B., Park-Min, K.-H., and Ivashkiv, L. B. (2016) Cutting edge: EZH2 promotes osteoclastogenesis by epigenetic silencing of the negative regulator IRF8. *J. Immunol.* **196,** 4452–4456 CrossRef Medline
35. Wyngaarden, L. A., Delgado-Olguin, P., Su, I. H., Bruneau, B. G., and Hopyan, S. (2011) Ezh2 regulates anteroposterior axis specification and proximodistal axis elongation in the developing limb. *Development* **138,** 3759–3767 CrossRef Medline
36. Schwarz, D., Varum, S., Zemke, M., Schöler, A., Baggiolini, A., Draganova, K., Koseki, H., Schübeler, D., and Sommer, L. (2014) Ezh2 is required for neural crest-derived cartilage and bone formation. *Development* **141,** 867–877 CrossRef Medline
37. Hemming, S., Cakouros, D., Codrington, J., Vandyke, K., Arthur, A., Zannettino, A., and Gronthos, S. (2017) EZH2 deletion in early mesenchyme compromises postnatal bone microarchitecture and structural integrity and accelerates remodeling. *FASEB J.* **31,** 1011–1027 CrossRef Medline
38. Lui, J. C., Garrison, P., Nguyen, Q., Ad, M., Keembiyehetty, C., Chen, W., Jee, Y. H., Landman, E., Nilsson, O., Barnes, K. M., and Baron, J. (2016) EZH1 and EZH2 promote skeletal growth by repressing inhibitors of chondrocyte proliferation and hypertrophy. *Nat. Commun.* **7,** 13685 CrossRef Medline
39. Mirzamohammadi, F., Papaioannou, G., Inloes, J. B., Rankin, E. B., Xie, H., Schipani, E., Orkin, S. H., and Kobayashi, T. (2016) Polycomb repressive complex 2 regulates skeletal growth by suppressing Wnt and TGF-β signalling. *Nat. Commun.* **7,** 12047 CrossRef Medline
40. Logan, M., Martin, J. F., Nagy, A., Lobe, C., Olson, E. N., and Tabin, C. J. (2002) Expression of Cre recombinase in the developing mouse limb bud driven by a Prxl enhancer. *Genesis* **33,** 77–80 CrossRef Medline
41. Rodda, S. J., and McMahon, A. P. (2006) Distinct roles for Hedgehog and canonical Wnt signaling in specification, differentiation and maintenance of osteoblast progenitors. *Development* **133,** 3231–3244 CrossRef Medline
42. Su, I. H., Basavaraj, A., Krutchinsky, A. N., Hobert, O., Ullrich, A., Chait, B. T., and Tarakhovsky, A. (2003) Ezh2 controls B cell development through histone H3 methylation and Igh rearrangement. *Nat. Immunol.* **4,** 124–131 CrossRef Medline
43. van Kemenade, F. J., Raaphorst, F. M., Blokzijl, T., Fieret, E., Hamer, K. M., Satijn, D. P., Otte, A. P., and Meijer, C. J. (2001) Coexpression of BMI-1 and EZH2 polycomb-group proteins is associated with cycling cells and degree of malignancy in B-cell non-Hodgkin lymphoma. *Blood* **97,** 3896–3901 CrossRef Medline
44. Bracken, A. P., Pasini, D., Capra, M., Prosperini, E., Colli, E., and Helin, K. (2003) EZH2 is downstream of the pRB-E2F pathway, essential for proliferation and amplified in cancer. *EMBO J.* **22,** 5323–5335 CrossRef Medline
45. Bachmann, I. M., Halvorsen, O. J., Collett, K., Stefansson, I. M., Straume, O., Haukaas, S. A., Salvesen, H. B., Otte, A. P., and Akslen, L. A. (2006) EZH2 expression is associated with high proliferation rate and aggressive tumor subgroups in cutaneous melanoma and cancers of the endometrium, prostate, and breast. *J. Clin. Oncol.* **24,** 268–273 CrossRef Medline
46. Comet, I., Riising, E. M., Leblanc, B., and Helin, K. (2016) Maintaining cell identity: PRC2-mediated regulation of transcription and cancer. *Nat. Rev. Cancer* **16,** 803–810 CrossRef Medline
47. Wassef, M., and Margueron, R. (2017) The multiple facets of PRC2 alterations in cancers. *J. Mol. Biol.* **429,** 1978–1993 CrossRef Medline
48. McGee-Lawrence, M. E., Carpio, L. R., Schulze, R. J., Pierce, J. L., McNiven, M. A., Farr, J. N., Khosla, S., Oursler, M. J., and Westendorf, J. J. (2016) Hdac3 Deficiency increases marrow adiposity and induces lipid storage and glucocorticoid metabolism in osteochondroprogenitor cells. *J. Bone Miner. Res.* **31,** 116–128 CrossRef Medline
49. Carpio, L. R., Bradley, E. W., McGee-Lawrence, M. E., Weivoda, M. M., Poston, D. D., Dudakovic, A., Xu, M., Tchkonia, T., Kirkland, J. L., van Wijnen, A. J., Oursler, M. J., and Westendorf, J. J. (2016) Histone deacetylase 3 supports endochondral bone formation by controlling cytokine signaling and matrix remodeling. *Sci. Signal.* **9,** ra79 CrossRef Medline
50. Addison, W. N., Fu, M. M., Yang, H. X., Lin, Z., Nagano, K., Gori, F., and Baron, R. (2014) Direct transcriptional repression of Zfp423 by Zfp521 mediates a bone morphogenic protein-dependent osteoblast versus adipocyte lineage commitment switch. *Mol. Cell Biol.* **34,** 3076–3085 CrossRef Medline
51. Liu, Y., Strecker, S., Wang, L., Kronenberg, M. S., Wang, W., Rowe, D. W., and Maye, P. (2013) Osterix-cre labeled progenitor cells contribute to the formation and maintenance of the bone marrow stroma. *PLoS One* **8,** e71318 CrossRef Medline

52. Chen, J., Shi, Y., Regan, J., Karuppaiah, K., Ornitz, D. M., and Long, F. (2014) Osx-Cre targets multiple cell types besides osteoblast lineage in postnatal mice. *PLoS One* **9,** e85161 CrossRef Medline
53. Pierce, J. L., Begun, D. L., Westendorf, J. J., and McGee-Lawrence, M. E. (2018) Defining osteoblast and adipocyte lineages in the bone marrow. *Bone* CrossRef Medline
54. Li, C., Chai, Y., Wang, L., Gao, B., Chen, H., Gao, P., Zhou, F. Q., Luo, X., Crane, J. L., Yu, B., Cao, X., and Wan, M. (2017) Programmed cell senescence in skeleton during late puberty. *Nat. Commun.* **8,** 1312 CrossRef Medline
55. Lee, S. T., Li, Z., Wu, Z., Aau, M., Guan, P., Karuturi, R. K., Liou, Y. C., and Yu, Q. (2011) Context-specific regulation of NF-κB target gene expression by EZH2 in breast cancers. *Mol. Cell* **43,** 798–810 CrossRef Medline
56. Xu, K., Wu, Z. J., Groner, A. C., He, H. H., Cai, C., Lis, R. T., Wu, X., Stack, E. C., Loda, M., Liu, T., Xu, H., Cato, L., Thornton, J. E., Gregory, R. I., Morrissey, C., *et al.* (2012) EZH2 oncogenic activity in castration-resistant prostate cancer cells is Polycomb-independent. *Science* **338,** 1465–1469 CrossRef Medline
57. Zhong, Y., Ye, Q., Chen, C., Wang, M., and Wang, H. (2018) Ezh2 promotes clock function and hematopoiesis independent of histone methyltransferase activity in zebrafish. *Nucleic Acids Res.* **46,** 3382–3399 CrossRef Medline
58. Schroeder, T. M., and Westendorf, J. J. (2005) Histone deacetylase inhibitors promote osteoblast maturation. *J. Bone Miner. Res.* **20,** 2254–2263 CrossRef Medline
59. McGee-Lawrence, M. E., Bradley, E. W., Dudakovic, A., Carlson, S. W., Ryan, Z. C., Kumar, R., Dadsetan, M., Yaszemski, M. J., Chen, Q., An, K. N., and Westendorf, J. J. (2013) Histone deacetylase 3 is required for maintenance of bone mass during aging. *Bone* **52,** 296–307 CrossRef Medline
60. Schneider, C. A., Rasband, W. S., and Eliceiri, K. W. (2012) NIH Image to ImageJ: 25 years of image analysis. *Nat. Methods* **9,** 671–675 CrossRef Medline
61. Samsonraj, R. M., Dudakovic, A., Zan, P., Pichurin, O., Cool, S. M., and van Wijnen, A. J. (2017) A versatile protocol for studying calvarial bone defect healing in a mouse model. *Tissue Eng. Part C Methods* **23,** 686–693 CrossRef Medline
62. Dudakovic, A., Camilleri, E., Riester, S. M., Lewallen, E. A., Kvasha, S., Chen, X., Radel, D. J., Anderson, J. M., Nair, A. A., Evans, J. M., Krych, A. J., Smith, J., Deyle, D. R., Stein, J. L., Stein, G. S., *et al.* (2014) High-resolution molecular validation of self-renewal and spontaneous differentiation in clinical-grade adipose-tissue derived human mesenchymal stem cells. *J. Cell Biochem.* **115,** 1816–1828 CrossRef Medline
63. Robinson, J. T., Thorvaldsdóttir, H., Winckler, W., Guttman, M., Lander, E. S., Getz, G., and Mesirov, J. P. (2011) Integrative genomics viewer. *Nat. Biotechnol.* **29,** 24–26 CrossRef Medline
64. Thorvaldsdóttir, H., Robinson, J. T., and Mesirov, J. P. (2013) Integrative Genomics Viewer (IGV): high-performance genomics data visualization and exploration. *Brief. Bioinform.* **14,** 178–192 CrossRef Medline
65. Ashburner, M., Ball, C. A., Blake, J. A., Botstein, D., Butler, H., Cherry, J. M., Davis, A. P., Dolinski, K., Dwight, S. S., Eppig, J. T., Harris, M. A., Hill, D. P., Issel-Tarver, L., Kasarskis, A., Lewis, S., Matese, J. C., Richardson, J. E., Ringwald, M., Rubin, G. M., and Sherlock, G. (2000) Gene ontology: tool for the unification of biology: the Gene Ontology Consortium. *Nat. Genet.* **25,** 25–29 CrossRef Medline
66. Carbon, S., Ireland, A., Mungall, C. J., Shu, S., Marshall, B., Lewis, S., AmiGO Hub, and Web Presence Working Group (2009) AmiGO: online access to ontology and annotation data. *Bioinformatics* **25,** 288–289 CrossRef Medline

Enhancer of zeste homolog 2 (*Ezh2*) controls bone formation and cell cycle progression during osteogenesis in mice

Amel Dudakovic, Emily T. Camilleri, Christopher R. Paradise, Rebekah M. Samsonraj, Martina Gluscevic, Carlo Alberto Paggi, Dana L. Begun, Farzaneh Khani, Oksana Pichurin, Farah S. Ahmed, Ranya Elsayed, Mohammed Elsalanty, Meghan E. McGee-Lawrence, Marcel Karperien, Scott M. Riester, Roman Thaler, Jennifer J. Westendorf and Andre J. van Wijnen

J. Biol. Chem. 2018, 293:12894-12907.
doi: 10.1074/jbc.RA118.002983 originally published online June 13, 2018

Enhancer of zeste homolog 2 (Ezh2) controls bone formation and cell cycle progression during osteogenesis in mice

Amel Dudakovic[1,2], Emily T. Camilleri[1], Christopher R. Paradise[3,4], Rebekah M. Samsonraj[1], Martina Gluscevic[3], Carlo Alberto Paggi[5], Dana L. Begun[1], Farzaneh Khani[1], Oksana Pichurin[1], Farah S. Ahmed[1], Ranya Elsayed[6], Mohammed Elsalanty[6], Meghan E. McGee-Lawrence[7,8], Marcel Karperien[5], Scott M. Riester[1], Roman Thaler[1], Jennifer J. Westendorf[1,2], Andre J. van Wijnen[1,2]*

[1]Department of Orthopedic Surgery, Mayo Clinic, Rochester, MN, USA
[2]Department of Biochemistry & Molecular Biology, Mayo Clinic, Rochester, MN, USA
[3]Mayo Clinic Graduate School of Biomedical Sciences, Mayo Clinic, Rochester, MN, USA
[4]Center for Regenerative Medicine, Mayo Clinic, Rochester, MN, USA
[5]Department of Developmental BioEngineering, University of Twente, Enschede, Netherlands
[6]Department of Oral Biology, Augusta University, Augusta, GA, USA
[7]Department of Cellular Biology and Anatomy, Medical College of Georgia, Augusta University, Augusta, GA, USA
[8]Department of Orthopedic Surgery, Medical College of Georgia, Augusta University, Augusta, GA, USA

Running title: Ezh2 function in proliferating osteoprogenitor cells

*To whom correspondence should be addressed: Andre J. van Wijnen, Ph.D., Departments of Orthopedic Surgery and Biochemistry & Molecular Biology, Mayo Clinic, 200 First Street SW, Rochester, MN 55905, USA, Tel.: (507) 293-2105; Fax: (507) 284-5075; E-Mail: vanwijnen.andre@mayo.edu

Suppl. Figure 1. Osteoblastic loss of Ezh2 reduces osteoclast numbers in adult animals. Static histomorphometric assessment for osteoblast surface (Ob.S, left) and osteoclast surface (Oc.S, right) in relationship to bone surface (BS). Analysis was performed on femurs from twelve week old male CON (n = 8) and Ezh2 cKO^{Osx} (n = 9) animals.

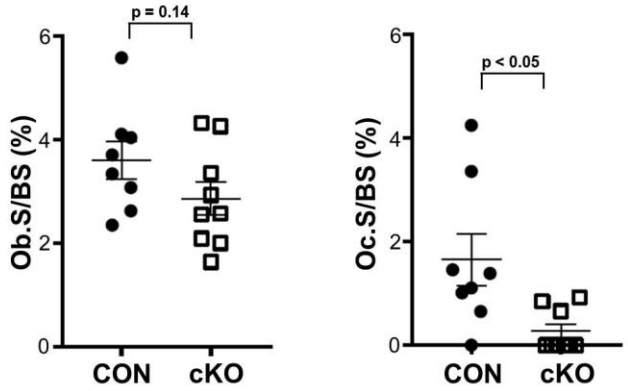

Suppl. Figure 2. Loss of Ezh2 reduces alkalike phosphatase activity in BMSCs. Alkaline phosphatase activity of BMSCs derived from male and female Control (CON) and Ezh2 cKO animals was perfomed on D8 of osteogenic differentiation.

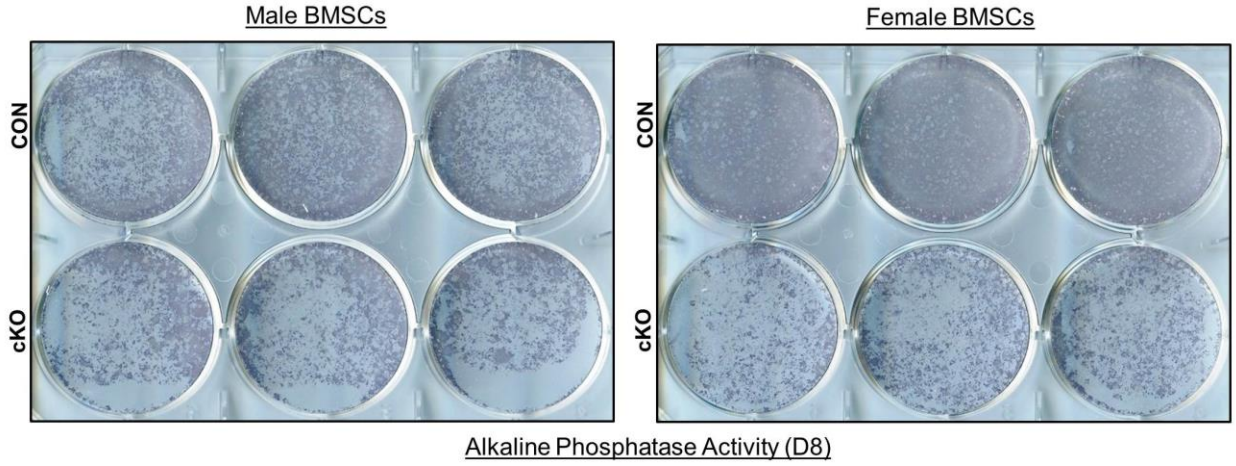

Suppl. Table 1. µCT cortical bone parameters.

	Animal #	Weight (g)	Ct.Ar (mm^2)	Ec.Ar (mm^2)	Ps.Ar (mm^2)	Md.Ar.Frac (%)	Ct.Po (%)	Ct.Th (mm)
3 Weeks								
CON	6	7.9 ± 0.8	0.17 ± 0.02	0.20 ± 0.04	0.40 ± 0.05	0.49 ± 0.05	0.005 ± 0.001	0.09 ± 0.01
cKO	6	7.4 ± 1.2	0.18 ± 0.03	0.20 ± 0.06	0.42 ± 0.09	0.48 ± 0.06	0.006 ± 0.004	0.10 ± 0.01
p-value		0.390	0.657	0.914	0.806	0.789	0.518	0.665
8 weeks								
CON	6	21.5 ± 0.8	0.56 ± 0.09	0.24 ± 0.03	0.80 ± 0.07	30 ± 5	0.20 ± 0.04	0.23 ± 0.03
cKO	6	21.2 ± 0.4	0.52 ± 0.04	0.24 ± 0.07	0.77 ± 0.09	31 ± 5	0.16 ± 0.02	0.22 ± 0.02
p-value		0.453	0.334	0.793	0.521	0.611	***0.038***	0.406
12 weeks								
CON	8	22.4 ± 1.5	0.50 ± 0.07	0.23 ± 0.06	0.79 ± 0.11	29 ± 5	0.18 ± 0.04	0.21 ± 0.03
cKO	9	22.6 ± 1.4	0.53 ± 0.05	0.20 ± 0.04	0.80 ± 0.06	25 ± 4	0.18 ± 0.03	0.23 ± 0.02
p-value		0.772	0.313	0.314	0.867	0.149	0.981	0.124

p-value calculated using Student's t-Test.

Suppl. Table 2. µCT trabecular bone parameters.

	Animal #	Weight (g)	tibia length	BV/TV (%)	Tb.N (1/mm)	Tb.Th (mm)	Tb.Sp (mm)	ConnD ($1/mm^3$)	SMI
3 Weeks									
CON	6	7.6 ± 0.5	12.1 ± 0.5	5.4 ± 1.6	1.8 ± 0.5	0.030 ± 0.005	0.15 ± 0.03	4720 ± 1890	2.5 ± 0.2
cKO	8	7.2 ± 1.1	12.1 ± 0.8	3.6 ± 1.1	1.2 ± 0.4	0.032 ± 0.003	0.18 ± 0.03	2655 ± 1159	2.7 ± 0.3
p-value		0.371	0.921	***0.026***	***0.015***	0.542	0.118	***0.026***	0.306
8 Weeks									
CON	9	22.0 ± 1.1	16.8 ± 0.3	8.0 ± 3.0	1.6 ± 0.5	0.050 ± 0.006	0.18 ± 0.04	2326 ± 1165	2.9 ± 0.2
cKO	10	20.6 ± 0.9	16.2 ± 0.6	5.8 ± 1.4	1.2 ± 0.2	0.047 ± 0.003	0.20 ± 0.03	1752 ± 325	2.9 ± 0.1
p-value		***0.006***	***0.021***	0.053	0.07	0.103	0.367	0.153	0.865
12 weeks									
CON	8	22.4 ± 1.5	16.7 ± 0.3	4.5 ± 1.9	0.80 ± 0.31	0.056 ± 0.005	0.30 ± 0.04	259 ± 137	2.8 ± 0.3
cKO	9	22.6 ± 1.4	16.4 ± 0.5	6.0 ± 3.1	0.98 ± 0.34	0.059 ± 0.008	0.28 ± 0.02	302 ± 136	2.8 ± 0.2
p-value		0.772	0.113	0.247	0.294	0.315	0.448	0.534	0.623

p-value calculated using Student's t-Test.

Suppl. Table 3. RT-qPCR primers.

GENE ID	FORWARD PRIMER	REVERSE PRIMER
Gapdh	CATCACTGCCACCCAGAAGACTG	ATGCCAGTGAGCTTCCCGTTCAG
Akt1	CACACGTCAAGCGACCCATGAA	TCTTCTCGCTCTCGTTCAGCAG
Ezh2	CATACGCTCTTCTGTCGACGATG	ACACTGTGGTCCACAAGGCTTG
Ezh2^{mut}	AAGCACAATGCAACACCAAA	TTCGATGCCCACATACTTCA
Ezh2^{SET}	CAACCCGAAAGGGCAACAAA	TTTCTCGTTCGATGCCCACA
Sp7	GGCTTTTCTGCGGCAAGAGGTT	CGCTGATGTTTGCTCAAGTGGTC
Bglap	GCAATAAGGTAGTGAACAGACTCC	CCATAGATGCGTTTGTAGGCGG
Ibsp	GAATGGCCTGTGCTTTCTCG	CCGGTACTTAAAGACCCCGTT
Alpl	CCAGAAAGACACCTTGACTGTGG	TCTTGTCCGTGTCGCTCACCAT
Runx2	CCTGAACTCTGCACCAAGTCCT	TCATCTGGCTCAGATAGGAGGG
Col1a1	CCTCAGGGTATTGCTGGACAAC	CAGAAGGACCTTGTTTGCCAGG
GFP	CACATGAAGCAGCACGACT	GGTCTTGTAGTTGCCGTCGT
Cre	ACCAGCCAGCTATCAACTCG	TTACATTGGTCCAGCCACC
Omd	TGCACATTCAGCAACTCAACC	TGCAGTCACAGCCTCAATGT
Eef1a1	CAACATCGTCGTAATCGGACA	GTCTAAGACCCAGGCGTACTT
Mki67	CAGAGCTAACTTGCGCTGAC	ACTACAGGCAGCTGGATACG
Ccnb2	GCACTACCATCCTTCTCAGGTG	TGTGCTGCATGACTTCCAGGAC
Cdkn2a (p16)	GGGTTTCGCCCAACGCCCCGA	TGCAGCACCACCAGCGTGTCC
Cdkn2a (p19)	GTTTTCTTGGTGAAGTTCGTGC	TCATCACCTGGTCCAGGATTC
Cdkn1a (p21)	GAACATCTCAGGGCCGAAAA	TGCGCTTGGAGTGATAGAAATC